Submitted to
Phys. Rev. C

LBL-1972
Preprint

c.1

A STUDY OF THE TWO PROTON TRANSFER REACTIONS $^{208}Pb(^{12}C, ^{10}Be)^{210}Po$ AND $^{208}Po(^{16}O, ^{14}C)^{210}Po$

F. D. Becchetti, D. G. Kovar, B. G. Harvey,
D. L. Hendrie, H. Homeyer, J. Mahoney,
W. von Oertzen, and N. K. Glendenning

August 1973

Prepared for the U. S. Atomic Energy Commission
under Contract W-7405-ENG-48

For Reference

Not to be taken from this room

RECEIVED
LAWRENCE
RADIATION LABORATORY

OCT 22 1973

LIBRARY AND
DOCUMENTS SECTION

LAWRENCE BERKELEY LABORATORY
UNIVERSITY OF CALIFORNIA
BERKELEY

LBL-1972

DISCLAIMER

This document was prepared as an account of work sponsored by the United States Government. While this document is believed to contain correct information, neither the United States Government nor any agency thereof, nor the Regents of the University of California, nor any of their employees, makes any warranty, express or implied, or assumes any legal responsibility for the accuracy, completeness, or usefulness of any information, apparatus, product, or process disclosed, or represents that its use would not infringe privately owned rights. Reference herein to any specific commercial product, process, or service by its trade name, trademark, manufacturer, or otherwise, does not necessarily constitute or imply its endorsement, recommendation, or favoring by the United States Government or any agency thereof, or the Regents of the University of California. The views and opinions of authors expressed herein do not necessarily state or reflect those of the United States Government or any agency thereof or the Regents of the University of California.

0 0 0 0 4 0 0 0 5 0 6

A STUDY OF THE TWO PROTON TRANSFER REACTIONS $^{208}Pb(^{12}C, ^{10}Be)^{210}Po$ AND $^{208}Po(^{16}O, ^{14}C)^{210}Po$*

F. D. Becchetti[†], D. G. Kovar[‡], B. G. Harvey, D. L. Hendrie,
H. Homeyer[‡], J. Mahoney, W. von Oertzen[‡] and N. K. Glendenning

Lawrence Berkeley Laboratory
University of California
Berkeley, California 94720

August 1973

ABSTRACT

Levels in ^{210}Po have been investigated using the two proton transfer reactions (^{12}C, ^{10}Be) and (^{16}O, ^{14}C) on ^{208}Pb at incident energies $E(^{12}C) = 78$ MeV and $E(^{16}O) = 104$ and 140 MeV. Reaction products were identified and energies measured with a magnetic spectrometer and a focal-plane resistive-wire proportional counter. Many previously unreported levels in ^{210}Po were observed. The results have been analyzed using DWBA, and shell model wave functions for levels in ^{210}Po have been tested. The $0^+ \rightarrow 0^+$(g.s.) transition is enhanced by a factor ~ 8 compared with the expected strength for a pure $(\pi h_{9/2})^2$ 0^+ configuration for ^{210}Po(g.s.).

I. INTRODUCTION

Many shell model calculations have been performed predicting levels in nuclei consisting of a few particles or holes outside of a ^{208}Pb core. Most of these nuclei can be studied with a variety of light ion reactions. To date, however, the levels in ^{210}Po formed by transferring two protons directly to the ^{208}Pb core have not been studied. In this paper we report the observation of levels in ^{210}Po via the heavy ion two-proton transfer reactions: (^{12}C, ^{10}Be) and (^{16}O, ^{14}C). The results are used to test predictions of available shell model wave-functions.

II. EXPERIMENTAL PROCEDURE

The experiments were performed using ^{12}C(E_L = 78 MeV) and ^{16}O(E_L = 104, 140 MeV) beams from the LBL 88-inch cyclotron. The beam was energy-dispersed across the target by a pair of analyzing magnets.[1] Reaction products were detected in the focal plane of a dispersion-matched magnetic spectrometer with a position-sensitive proportional counter (6 horizontal wires, 6 x 45 cm effective area) backed by a plastic scintillator.[2] A schematic diagram of the apparatus is shown in Figure 1. The focal plane counter is described in detail elsewhere.[2,3] The counter system measures Bρ (position), energy loss (ΔE/ΔX), time-of-flight (TOF) and a scintillator output (energy) for heavy ion reaction products. This information is sufficient to give unambiguous particle identification. In the present arrangement a time-zero detector[4] consisting of a thin (∿ 80 μg/cm^2) NE111 plastic scintillator was placed at the entrance of the spectrometer (see Figure 1). The signal from this detector and another from the final scintillator were used for the TOF measurement (replacing the cyclotron rf signal employed previously[2]). Typical

resolutions (FWHM) in the present experiment were $\Delta E/\Delta X \sim 10\%$, TOF $\sim 1\%$ (2.5 nsec.)* and energy resolution $\delta E/E \sim 0.15\%$ or approximately 100-150 keV for (^{12}C, ^{10}Be) and 120-200 keV for (^{16}O, ^{14}C), depending on the target thickness. Charge and mass separation up to $A \sim 20$ was obtained. A two-dimensional spectrum of $\Delta E/\Delta X$ vs. TOF is shown in Figure 2. Energy spectra for different particle groups are obtained by setting gates on $\Delta E/\Delta X$ and TOF.[2,3]

Both "thin" ($\sim 100\ \mu g/cm^2$) and "thick" ($\sim 300\ \mu g/cm^2$) targets consisting of ^{208}Pb evaporated onto thin carbon foils (10-30 $\mu g/cm^2$) were used. Some of the targets also had a layer of carbon evaporated over the ^{208}Pb so as to reduce evaporation and sputtering of the ^{208}Pb from beam bombardment. In order to reduce the latter effects we limited the beam currents to $\lesssim 300$ na (fully stripped ions).

Cross sections were obtained from the particle yields relative to a monitor counter and the $^{16}O(8^+)$ yield, which in turn, was normalized to Rutherford cross sections at forward angles. The targets were orientated such that reaction products exited through a thickness of carbon sufficient to ensure charge equilibrium. Measurements of yields to various charge states indicated that the reaction products were predominantly ($\geq 80\%$) fully stripped. Therefore cross sections were calculated from the measured yields of the fully stripped ions, corrected by an appropriate factor.[3]

The energy calibration of the focal plane counter was obtained by sweeping elastically scattered particles across the detector by varying the spectrometer field in known steps. The results were parametrized in such a way that the energy of any particle could be determined from its position

*The TOF resolution is limited by the differences in particle flight paths through the spectrometer.

measurement to an accuracy $\sim \pm .05\%$ ($\pm$ 30 to $\pm$ 70 keV). The data used to obtain the energy calibration were also used to generate parameters which allowed position spectra from the six individual wires to be added together to form a single spectrum.

Several spectra were obtained using thin targets ($\sim$ 100 $\mu g/cm^2$) to accurately determine the position and relative intensity of levels. Thick targets ($\sim$ 300 $\mu g/cm^2$) were then used to obtain angular distributions.

III. EXPERIMENTAL RESULTS

A. Spectra

Particle spectra obtained for the reactions $^{208}Pb(^{12}C, ^{10}Be)^{210}Po$, $E(^{12}C)$ = 78 MeV and $^{208}Pb(^{16}O, ^{14}C)^{210}Po$, $E(^{16}O)$ = 104 MeV are shown in Figures 3-4. The ^{12}C and ^{16}O bombarding energies correspond to the same projectile velocities and nearly the same energy above the Coulomb barrier ($\sim$ 20 MeV greater). In Figure 4 the angle (52.5° lab) is near the peak in the measured angular distributions, which are similar for the two reactions or different levels (see Section III.B). Shown in Figure 5 is a ^{14}C spectrum for $^{208}Pb(^{16}O, ^{14}C)^{210}Po$ at $E(^{16}O)$ = 140 MeV. Although the energy resolution is poorer at the higher combarding energy, one observes that most of the states seen at $E(^{16}O)$ = 104 MeV are populated.

The shapes of the spectra shown in Figures 3-5 reflect the strong Q-value dependence of heavy-ion reactions.[5,6] This dependence results in a "Q-window" whose centroid, Q_{opt}, depends on the charge transfer and bombarding energy.[5] Semi-classical theory[5] predicts for sub-Coulomb reactions $Q_{opt} \approx E_1(Z_t/Z_1)$ where E_1 is the incident c.m. energy, Z_t is the charge transferred to the projectile, and Z_1 is the projectile charge (assumed here

to be much smaller than the target charge). This gives $Q_{opt} \approx -25$, -24 and -33 MeV or $E_x = 6.6$, 10.4 and 19.4 MeV for $^{208}Pb(^{12}C, ^{10}Be)$, $E_L = 78$ MeV and $^{208}Pb(^{16}O, ^{14}C)$, $E_L = 104$ and 140 MeV, respectively. No-recoil DWBA calculations ($L \sim 0$), however, give $Q_{opt} \approx -14$ MeV for all of these reactions or $E_x \approx 0$-2 MeV (see Section V.C).

The data appear to indicate $E_x \approx 4$, 7.5 and 15 MeV, respectively, i.e., the observed Q_{opt} values are slightly more positive than those given by the semi-classical approximation and considerably more negative than those given by DWBA. The exact shapes of the spectra, however, are complicated functions of both the Q-dependence of the reaction and the structure of the final states. Recoil effects are also important (see Section 3, Appendix).

The particle groups observed in the present experiment and their partial integrated cross sections are presented in Table I. The groups listed can in principle consist of both ^{210}Po and the outgoing products (^{14}C and ^{10}Be) being in particle-stable excited states. ^{10}Be has such known[8] levels $E_x(J^\pi) = 3.37(2^+)$, $5.96(1^-,2^+)$, $6.18(0^+)$ and $6.26(2^-)$ MeV while for ^{14}C (ref. 9): $E_x(J^\pi) = 6.09(1^-)$, $6.59(0^+)$, $6.73(3^-)$, $6.90(0^-)$, $7.01(2^+)$ and $7.34(2^-)$ MeV. Groups from outgoing particles in excited states have been observed in (^{16}O, ^{15}N) and (^{12}C, ^{11}B) at $E_L = 104$ MeV and 78 MeV on Zr and Mo targets and are observed to be substantially (200-700 keV) broadened, apparently by gamma decay in flight.[3] A comparison of the position and widths of levels observed in the different reactions indicates that groups seen with $E_x < 5.5$ MeV are due to levels in ^{210}Po, with the exception of a group seen in (^{12}C, ^{10}Be) at $E_x = 3.41$ MeV which could be $^{10}Be^*$ (3.37 MeV). The weak intensity seen would be consistent with the results of a $^{18}O(^{12}C, ^{10}Be)^{20}Ne$ experiment[10] in which this level was not populated. There are indications,

however, that some groups with $E_x > 6$ MeV observed in (^{16}O, ^{14}C) are due to excitation of ^{14}C (see Figures 3-5), particularly the group of "levels" at $E_x \sim 7$ MeV.

B. Angular Distributions

Angular distributions are shown in Figures 6-7. A few forward angle points for some of the levels observed in (^{16}O, ^{14}C) were obscured by contaminants. The error bars shown reflect only the statistical errors (std. dev.) in the estimated total yield and background correction. The fluctuations in the data at $E_x > 6$ MeV may not be significant owing to the level density and background at high excitation.

The shapes of the angular distributions for $E_x < 6$ MeV are essentially the same to within the errors indicated even though known states of very different spins ($J^\pi = 0^+$ to 8^+) are shown (see Section IV). This lack of "J-signature" has been noted previously for (^{16}O, ^{15}N) etc. on heavy target nuclei[11] and greatly limits the usefulness of heavy ion reactions in extracting spins for these nuclei. As observed in a comparison of the $^{208}Pb(^{12}C, ^{11}B)^{209}Bi$ and $^{208}Pb(^{16}O, ^{15}N)^{209}Bi$ reactions[11] it may be possible to obtain spectroscopic information from the comparison of heavy ion reactions involving different projectiles. As seen in Figure 4 there are some notable differences in the spectra shown, e.g. the population of the levels at $E_x = 3.7$ and 4.0 MeV. We discuss this further in Section V.E.

IV. KNOWN LEVELS IN ^{210}Po

The low lying levels in ^{210}Po have been studied previously by several means: (i) the decay of ^{210}At (ref. 13); (ii) the ^{208}Pb (α, 2n-γ) reaction[14,15]; (iii) inelastic scattering[16] and proton pickup[17] from ^{210}Po; and (iv) the (α,t) and (^3He,d) reactions[18,19] on ^{209}Bi.

Of these studies (iv) is of most interest here since $^{209}Bi(\alpha,t)$ and $^{209}Bi(^{3}He,d)$ should populate states of the form $[\pi\ell j \otimes \pi\, h_{9/2}]_J$ outside of a ^{208}Pb core. It is also possible to reach such states via the heavy ion reactions $(^{12}C,\ ^{11}B)$ and $(^{16}O,\ ^{15}N)$. In Figure 8 we compare the results[18,19] of $^{209}Bi(\alpha,t)^{210}Po$ and $^{209}Bi(^{3}He,d)^{210}Po$ with spectra from $(^{12}C,\ ^{11}B)$ and $(^{16}O,\ ^{15}N)$. It can be seen that the heavy ion reactions populate the same levels as in (α,t) and $(^{3}He,d)$ (although adjacent members of a multiplet are not always resolved). In Table II we list the levels in ^{210}Po believed[18,19] to be $[\pi\ell j \otimes \pi\, h_{9/2}]$ and compare calculated spectroscopic factors relative to those of single particle states in ^{209}Bi observed[11] in $^{208}Pb(^{12}C,\ ^{11}B)$ and $^{208}Pb(^{16}O,\ ^{15}N)$ at the same bombarding energies. The results are consistent with the light ion results[18,19] and we therefore conclude that the heavy-ion reactions proceed via a direct single-step transfer without appreciable core-excitation. As in the reaction[11] $^{208}Pb \rightarrow {}^{209}Bi$ we observe a j-selectivity which depends on the structure of the projectile. The $(^{16}O,\ ^{15}N)$ reaction $(n\ell j = 1p_{1/2})$ favors final states involving transitions with the single particle orbits $j = \ell + 1/2$ compared to $(^{12}C,\ ^{11}B)$ $(n\ell j = 1p_{3/2})$. Furthermore, single particle wave functions with large radial extension (large n) are favored.

The known levels in ^{210}Po and some of their properties are given in Table III. The levels observed in $^{209}Bi(\alpha,t)^{210}Po$ and $^{209}Bi(^{3}He,d)$ are also indicated in Figures 4 and 8.

V. DWBA CALCULATIONS

A. Cross Section

Since kinematic effects play a dominant role in heavy ion reactions, it is necessary to account for these before attempting to deduce spectroscopic

information. Fortunately DWBA theory appears to reproduce kinematic effects reasonably well[6], although some details remain questionable.[11,21,22]

The cross section for the transfer of two identical nucleons from spinless projectiles, A(a,b)B where a = b + 2 and B = b + 2, can be written in the "no-recoil" approximation (see Appendix) as[23,24,25]

$$\frac{d\sigma}{d\Omega} = \frac{2J_B + 1}{2J_A + 1} \frac{d\sigma^{DW}}{d\Omega} (\theta) \quad . \tag{1}$$

J_A and J_B are the initial and final target spins, respectively. In the special cases considered here ($J_a = J_b = 0$, $\Delta T = 1$ and $\Delta S = 0$) we have $J_A = 0(\pi_i = +)$ so that $L = J = J_B$ and $\pi_f = (-1)^L$, i.e. only transitions to states of natural parity are allowed.

B. Form Factors

Various methods have recently been devised to calculate the form factors for heavy ion two-nucleon transfers.[26-30] The problem is substantially more complicated than for light ion reactions such as (t,p) etc. since a zero-range interaction would not be appropriate for projectiles such as ^{16}O and ^{12}C. In addition, the transferred nucleons occupy single particle states other than $1s_{1/2}$ as in light ions such as t and α and therefore the relative motion of these nucleons may be more complex.

We have used two methods to calculate form factors. Both methods are applicable for the simultaneous transfer of two nucleons (in contrast to a sequential transfer). One method computes the form factor as a matrix element of the sum of the shell model interactions that bind the transferred nucleons to the projectile core. We refer to this as the "sum of interactions" (SI). The other method approximates the sum of the

interactions by a single potential acting on the center of mass of the transferred nucleons. We refer to this as the "center-of-mass interaction" (CMI). Both the CMI and SI methods yield a local form factor which depends only on the separation, R, between projectile and target core, and the angular momentum transfer. Thus Eq. (1) can be calculated with conventional "no-recoil" DWBA programs. Corrections to DWBA due to recoil can also be included, as described in the Appendix (Section 3).

1. Center-of-Mass Interaction (CMI)

The CMI method is an extension of the method used by Glendenning[25] to treat (p,t), (t,p), (^{3}He,n), etc. Since the interaction involves only the center-of-mass (c.m.) coordinates its matrix elements can be computed by transforming the coordinates of the two nucleons in the projectile and target into relative and c.m. motion with the aid of the Moshinsky-Talmi expansion.[31] The c.m. motion is approximated by Hankel functions and the Buttle-Goldfarb[5] method used to obtain the asymptotic part of the form factor as a function of R. The interaction inducing the transition is that acting on the c.m. of the two nucleons in the projectile a = b + 2 (post representation). Details are given in the Appendix and reference 26. The results are[26]

$$F_L(R) \rightarrow \left\{ \Sigma\, \Omega_{12}\, G_1\, G_2\, N_{N_2\Lambda_2}\, A_{N_1\Lambda_1} \right\} h_L^{(1)*}(i\kappa R) \tag{2a}$$

$$\doteq \quad f_L\, h_0^{(1)*}(i\kappa R) \tag{2b}$$

where Ω_{12} is an overlap integral, G_1 (G_2) are the projectile (target) structure factors and $N_{N_2\Lambda_2}\, A_{N_1\Lambda_1}\, h_L^{(1)*}(i\kappa R)$ is a projection of the asymptotic part of the c.m. motion of the transferred nucleons onto the projectile-target core separation, R. The summation indicated in Eq. (2a) is over all allowed states of relative and c.m. motion (see Appendix).

Although Eqs. (2a and 2b) are valid only in the asymptotic region, this is often adequate to describe reactions even at energies well above the Coulomb barrier owing to the strong absorption of the projectile for close encounters (see Section C.2).

The form factor (2a) is similar to that used in light-ion reactions[25], except that the structure of the projectile appears explicitly. As pointed out previously[26], the transfer process indicated by (2a) involves structure factors for the stripping of two nucleons from the projectile and the simultaneous pickup of these by the target.

In the transfer of two identical nucleons from $1s_{1/2}$ orbitals [such as (^{3}He,n)] only the relative 1S state of motion is available to the transferred nucleons. In contrast, for transfer of two identical nucleons from the 1p orbitals, relative motions in the 1S, 2S and 1P states are allowed. Owing to antisymmetrization, the 1S and 2S states are spin singlet while the 1P state is spin triplet. Although the 2S and 1P states are allowed and must be included in the form factor calculation, the strong transitions proceed predominantly by transfer via a relative 1S state (see Appendix).

Although there are now methods which do not require as many restrictive assumptions as the CMI method does, the decomposition indicated by (2a) often is very useful.

2. Sum of Interactions (SI)

A more basic formulation of the transfer process involves the matrix element of the interaction of each transferred nucleon with the projectile core (post representation). Thus if the interaction of the nucleons p and p' (see Figure 21) in a (= b + 2) with the core b is denoted by the shell model

potentials $V_1(r_1)$ and $V_1'(r_1')$, then the transition amplitude involves the matrix element $\langle A,a|V_1(r_1) + V_1'(r_1')|B,b\rangle$. This matrix element is integrated over all internal coordinates and the result is a function of the separation R between the cores A and b, and of the transferred angular momentum, L. Specific details of the SI method are given in the literature.[26,29,30]

Form factors for $^{208}Pb(^{12}C, {}^{10}Be)^{210}Po\ (0^+)$ obtained with the SI method are shown in Figure 9. The single particle wave functions have been calculated at a single, fixed binding energy in a Woods-Saxon well with $R = 1.20A^{1/3}$ fm, a = 0.60 fm, V_{SO} = 8 MeV and V adjusted. At large core separations, wave functions ($n\ell j$) with many nodes (large n) and yielding large relative 1S components (small ℓ) are favored for a given L transfer. The effect of nuclear structure (projectile and target) will be discussed in Section E.

3. Comparison of SI and CMI Methods

A detailed comparison of the SI and CMI methods as applied to two proton transfers may be found in the Appendix. Both methods give the same qualitative results although quantitative differences exist. These differences are greatest when the transfer proceeds by states having small relative 1S motion (e.g., $0^+ \rightarrow (1h_{9/2})^2\ 0^+$). A comparison of various methods as applied to two neutron transfers may be found in reference 26.

C. Kinematic Effects

1. Q-Windows

We can separate kinematic effects from nuclear structure by using the relation (see Appendix)

$$\frac{d\sigma}{d\Omega} \doteq |f_L|^2\ \sigma_L^{DW}\ (\theta) \qquad (3)$$

where f_L is a structure amplitude and $\sigma_L^{DW}(\theta)$ is the DWBA cross section calculated for a fixed form factor $h_0^{(1)*}(i\kappa R)$ $(= e^{-\kappa R}/\kappa R)$. The quantity κ is obtained by fitting a Hankel function to the asymptotic part of the form factor. Note that our definition of σ_L^{DW} in Eq. (3) includes the appropriate spin factors, e.g. $(2J_B + 1)$, contained in the general expression Eq. (2).

We have performed calculations for (^{12}C, ^{10}Be) and (^{16}O, ^{14}C) vs. Q and L. The DWBA program DWUCK[23] was used with a form factor $e^{-\kappa R}/\kappa R$, $\kappa = 1.6\ fm^{-1}$. Optical model parameters which fit the elastic scattering $^{16}O + {}^{208}Pb$ ($E_L = 104$ MeV) and $^{12}C + {}^{208}Pb$ ($E_L = 78$ MeV) were used[11]: $V = -40$ MeV, $W = -15$ MeV, $R = 1.31\ (A_1^{1/3} + A_2^{1/3})$ fm and $a = 0.45$ fm. The DWBA angular distributions are bell-shaped and peaked at an angle which changes with Q, but is nearly independent of L. The peak cross sections vs. excitation in the residual nucleus, E_x, and L are shown in Figures 10-11. The calculated Q-windows are essentially the same for the two reactions but owing to the differences in g.s. Q-values shift the curves to different E_x values. Inclusion of recoil shifts the Q windows ~ -4 MeV (see Appendix).

The general features are those expected from semi-classical theory[32,33,34]: a gaussian window centered about some Q_{opt} with width $\propto L$. The calculated Q_{opt} values (~ -14 MeV) are less negative than given by the sub-Coulomb formula of Buttle-Goldfarb[5] ($Q_{opt} \sim -25$ MeV). Also, the Q-windows appear to be much wider at higher bombarding energies, in agreement with semi-classical theory.[32,33,34] The quantity σ_L^{DW} (which includes $2J_B + 1 = 2L + 1$) increases rapidly with L only for $L \lesssim 6$. States with higher spin ($L > 6$) are therefore not particularly favored kinematically.

Similar features to those noted above are found for single nucleon transfers.[35]

2. Localization in R- and ℓ-Space

As will become apparent shortly, it is useful to calculate the localization of the (^{16}O, ^{14}C) and (^{12}C, ^{10}Be) reactions in terms of R and ℓ, the projectile-target core separation and relative angular momentum, respectively. The results of this are shown in Figures 12-13 where we consider the $^{208}Pb(^{12}C, ^{10}Be)^{210}Po$ (g.s.) L = 0 transition. The form factor consists of a mixture of the configurations shown in Figure 9. In Figure 12 we display the square of the matrix elements $\beta_L^M(\ell)$ as defined by Kunz[22] vs. ℓ for L=M=0. The most important contributions occur for a narrow region of ℓ-space centered at $\ell \sim 37\hbar$ which is about $10\hbar$ smaller than the classical ℓ-value calculated from the grazing angle, θ_{gr}, assuming Coulomb trajectories [$= \bar{\eta} \cot \theta/2$ where $\bar{\eta} = 1/2\ (\eta_i + \eta_f)$]. This difference reflects the influence of the attractive nuclear potential. In Figure 13 we show the square of the integrand of the radial integrals vs. R for $\ell = 37\hbar$. The largest contribution comes from a region near R = 12.3 fm. This is $\sim$ 1.5 fm (10%) smaller than the classical apsidal distance $D_{gr}^{c\ell}$ [$= (\bar{\eta}/\bar{k})(1 + \csc \theta_{gr}/2)$] and again demonstrates the effect of the nuclear potential.

A comparison of the theoretical curves of Figures 9 and 13 indicates that transfer cross sections are determined primarily by a narrow region of the asymptotic part of the form factor. We find that to a good approximation ($\lesssim$ 20%) relative transfer cross sections can be estimated by

$$\frac{d\sigma}{d\Omega} \propto |F_L(R_m)|^2\ \sigma_L^{DW}\ (\theta) \qquad (4)$$

where $F_L(R_m)$ is the form factor at some radius ($R_m \doteq 12$ fm) and σ_L^{DW} (θ) is

the cross section for a fixed form factor. We have used Eq. (3) extensively to estimate cross sections with $\sigma_L^{DW}(\theta)$ interpolated from calculations and $|F_L(R_m)|^2$ determined using either the CMI or SI methods.

D. Angular Distributions

We have calculated angular distributions for (^{12}C, ^{10}Be) and (^{16}O, ^{14}C) using the DWBA program DWUCK with form factors calculated with both CMI and SI methods, the former with a radial cut off at 8.5 fm (see Appendix). Some of the calculations are shown in Figures 6-7 (SI form factor). The calculated shapes of the angular distributions are nearly independent of L or the nuclear configurations. The maxima in the DWBA angular distributions shift back in angle with increasingly negative Q-value whereas the experimental results do not. This is shown in Figure 14 where we plot the calculated (CMI method) and observed peak angle in the cross sections. The latter were determined by shifting the calculated curves by eye to fit the data. Results similar to those shown in Figures 6, 7 and 14 have also been observed for single nucleon transfers on ^{208}Pb, refs. 11 and 12, and other mass regions.[36,37,38] The discrepancies between theory and experiment appear to be associated with the optical model description of the distorted waves in DWBA, since the quality of the fits are correlated[36] with projectile orbit mismatch ($Q-Q_{opt}$) as can be noted in Figures 6, 7 and 14 ($Q_{opt} \sim -14$ MeV).

The calculations can be brought into better agreement with experiment by adjusting optical model parameters[37], e.g. decreasing the half radius, R, by ~ 0.6 fm. The resulting parameters do not then fit the measured elastic scattering of ^{16}O and ^{12}C from ^{208}Pb. We have therefore chosen, instead, to use optical parameters which fit the elastic scattering in the incident channels and compare the DWBA calculations with integrated or peak cross sections.

One of the effects not included in the DWBA calculations is that due to recoil (see Appendix). Such effects are found to be important for certain types of single nucleon transfers between heavy ions where L transfers are restricted by a parity rule arising from the no-recoil assumption. The L-transfer for two-proton transfers with $J_a=J_b=J_A=0$, however, are a priori restricted to $L = J_B$. Recoil, then, alters the DWBA amplitude in the manner suggested by Buttle and Goldfarb[20] and should be minimal when $Q \approx Q_{opt}$. We have estimated recoil effects by comparing "no-recoil" and "recoil" DWBA calculation for a di-nucleon cluster transfer (Section 3, Appendix). The shapes of the angular distributions are not drastically altered by the inclusion of recoil, i.e., the discrepancies vs. Q value persist.

E. Sensitivity to Nuclear Structure

1. Projectile Dependence

It is a distinguishing feature of heavy ion reactions that the nucleons transferred to and from the projectile can be in single particle states other than $1s_{1/2}$. This feature can result in a j-selectivity such as that observed[11] in the (^{12}C, ^{11}B) and (^{16}O, ^{15}N) reactions. In (^{12}C, ^{11}B) the proton is transferred from a $1p_{3/2}$ orbit, i.e. a $j_>$ state ($\equiv \ell + 1/2$) whereas in (^{16}O, ^{15}N) the orbit is $1p_{1/2}$, a $j_<$ orbit. This results in constraints on the allowed L transfer which together with the Q and L-dependence of the cross sections leads to marked differences in the spectra observed for these reactions.[11] The following features are observed[11]: (^{16}O, ^{15}N) favors $j_>$ final states, i.e. a transition from a $j_<$ projectile state to a $j_>$

final state is preferred, whereas for (^{12}C, ^{11}B), a $j_>$ projectile, the $j_>$ and $j_<$ target states are populated with comparable intensities (see Figure 8).

Similarly one might expect a j-selectivity for two-nucleon transfers from ^{16}O and ^{12}C. In the two-nucleon transfers considered here, however, such effects must enter via the structure factors Eq. (2a) rather than constraints on L since $J_a = J_b = 0$. We have considered projectile wave functions consisting of a 0^+ core plus two protons in the $1p_{3/2}$ and $1p_{1/2}$ shell, i.e. $\alpha\ 1p^2_{3/2} + \beta\ 1p^2_{1/2}$ where $\alpha^2 + \beta^2 = 1$. The form factor for transitions to final states of the form $(n\ell j)^2\ 0^+$ have then been calculated (SI method) vs. the $(p_{1/2})^2$ mixing amplitude, β^2. The results are shown in Figure 15. At the top of Figure 15 we indicate mixing ratios contained in various shell model wave functions for two protons in ^{16}O and ^{12}C. These are: (1) pure jj-coupling ($\beta^2 = 0$ and 1), (2) pure LS-coupling ($\beta^2 \doteq 0.33$), and (3) Cohen-Kurath wave functions[39,40] (CK ^{12}C, and CK ^{16}O, $\beta^2 \doteq 0.24$ and 0.80, respectively). One observes the following preferred $0^+ \rightarrow 0^+$ transfers:

$$(j^2_>)_{0^+} \text{ projectile configuration} \rightarrow (j^2_<)_{0^+} \text{ target configuration} \qquad (5a)$$

and

$$(j^2_<)_{0^+} \text{ projectile configuration} \rightarrow (j^2_>)_{0^+} \text{ target configuration} \qquad (5b)$$

Thus transitions involving pure jj-coupled wave functions (projectile and target) should exhibit a pronounced projectile dependence analogous to that observed for some single nucleon transfers[11] (although the origin of the two effects are somewhat different).

Most of the j-selectivity indicated by Eqs. (5a and 5b) is destroyed by small amounts of configuration mixing in the projectile wave functions. Thus, e.g., a 20% admixture of $(p_{3/2})^2$ in ^{16}O increases the (^{16}O, ^{14}C) cross

sections to $j_<^2$ final states ($3p_{1/2}^2$, $2f_{5/2}^2$, $1h_{9/2}^2$) by factors of 4 to 200. Even with "realistic" projectile wave functions[39], however, measurable differences (~ 2) still exist between the calculated (^{12}C, ^{10}Be) and (^{16}O, ^{14}C) transition strengths.

2. Target-State Dependence

The low-lying states of ^{210}Po populated in two-proton transfers on ^{208}Pb are expected to consist of levels formed by two protons in the shell model orbits $n\ell j = 1h_{9/2}$, $2f_{7/2}$, $1i_{13/2}$, $2f_{5/2}$, $3p_{3/2}$ and $3p_{1/2}$. All states thus formed have positive parity except those involving the $1i_{13/2}$ "intruder" level from the next higher oscillator shell.

We have calculated the relative peak cross sections to these levels (SI method) with the aid of approximation (4). Cohen-Kurath wave functions (set a) were used for the projectiles.[39,40] The results are shown in Figures 16 and 17 where we display calculated peak cross sections (no-recoil DWBA) for (^{12}C, ^{10}Be) and (^{16}O, ^{14}C) vs. J, the spin of the final state in ^{210}Po. The final states $[n\ell j \otimes n'\ell'j']_J$ have been denoted by ℓ and j, e.g. $f_> \equiv f_{7/2}$ (= a $j_>$ state); $f_< \equiv f_{5/2}$ (= a $j_<$ state), etc.

The calculated cross sections vs. J will increase or decrease with increasing J depending on the j-values of the single-nucleon shell model orbits. Two types of transitions are noted:

$$\text{Type I:} \quad 0^+ \text{ (target)} \rightarrow [j_> \otimes j'_>]_J \text{ or } [j_< \otimes j'_<]_J \tag{6a}$$

and

$$\text{Type II:} \quad 0^+ \text{ (target)} \rightarrow [j_> \otimes j'_<]_J \text{ or } [j_< \otimes j'_>]_J \tag{6b}$$

Type I transitions are characterized by decreasing cross section with increasing J (within a multiplet) whereas Type II transitions exhibit the

opposite behavior. The relative strength between different multiplets depends on the projectile, with a preference similar to that noted for the 0^+ states Eqs. (5a and 5b). The J-dependence of the type I and II transitions Eqs. (6a and 6b) is directly related to the relative 1S, singlet spin, motion in the ^{210}Po wave functions. In both types of transitions 1S relative motion is maximum for the co-planar orbits J=j+j' or j-j', but for type I singlet spin requires J=j-j' and for type II, J=j+j'. This feature is not unique to heavy ion reactions. In fact, the structure factors for (^{12}C, ^{10}Be) (CMI method) are very similar to those[41] for (^{3}He,n) since the CK wavefunctions for ^{12}C are predominantly LS-coupled with a large relative 1S component. Thus, outside of differences due to kinematic effects, we would expect (^{12}C, ^{10}Be) and to some extent (^{16}O, ^{14}C) to populate the same state as in (^{3}He,n). This is discussed in more detail in the Appendix.

It is apparent from Figures 15 and 16 that (^{12}C, ^{10}Be) and (^{16}O, ^{14}C) reaction are selective. Out of the 52 states considered only 14 states are calculated to have strength $\geq$ 10% of the strongest transition ($0^+ \rightarrow f_{7/2}$ $p_{3/2}$ 2^+). The strongest transitions are those involving the $2f_{7/2}$ and $3p_{3/2}$ single particle orbits (low ℓ, large n).

VI. COMPARISON WITH EXPERIMENT: TEST OF SHELL MODEL WAVE FUNCTIONS FOR ^{210}Po

A. Spectra and Angular Distributions

In Section D.2 above we considered pure shell model configurations for ^{210}Po. Calculations[42-44] and experiments[13-19] indicate, however, that configuration mixing must be included. We have investigated two shell model calculations for ^{210}Po: that of Kuo-Herling (KH) which uses matrix elements deduced

from nucleon-nucleon scattering[43], and that of Ma-True (MT), which uses matrix elements calculated from a phenomenological force[44] (central + multipolar). Both calculations reproduce many of the properties for nuclei A $\sim$ 208: energy levels, spectroscopic factors, transition rates, etc. In Figure 18 we compare schematically predictions for levels in ^{210}Po with previously reported levels[13-19] and groups seen in the present experiment. Figures 19 and 20 compare the experimental spectra for (^{12}C, ^{10}Be) and (^{16}O, ^{14}C) with calculations (SI method and Eq. 4) using CK wave functions for the projectiles and MT wave functions for ^{210}Po. We have included a correction for recoil effects in the calculations (see Section 3, Appendix). The qualitative features of the spectra are reproduced, i.e., the number of levels and the distribution of transition strength, although the g.s. strength appears to be overestimated. As indicated in Figures 16 and 17, relatively few configurations dominate: $(f_{7/2}p_{3/2})$, $(f^2_{7/2})$, $(f_{7/2}i_{13/2})$, $(f_{7/2}p_{1/2})$, $(f_{7/2}f_{5/2})$, with the strengths spread via configuration mixing. There appear to be more than one candidate for each observed level $E_x > 2$ MeV, however, and unfortunately, the calculated angular distributions are nearly independent of J. This is shown in Figures 6 and 7 where we compare DWBA calculations with experiment (SI method, CK and MT wave functions). The DWBA curves shown have been calculated for the strongest transition indicated in Figures 15 and 16 using the SI form factor and are normalized to the peak cross-section. As noted in Section C.3 the calculated curves have approximately the correct (L-independent) shapes, but the peak positions shift with Q-value (or E_x) much faster than the data indicate (see Figure 14). The lack of appreciable L-signature makes it difficult to make specific level assignments which are not very model dependent. The projectile and final-state selectivity noted by Eqs. (5a-5b) can be utilized to suggest the likely spin and configuration for a given level. In Section VI

we will enumerate the likely candidates for the levels observed in (^{16}O, ^{14}C) and (^{12}C, ^{10}Be). These candidates are indicated in Figure 18.

B. Ground State Band

1. Relative Intensities

The 0^+ g.s., 2^+ (1.18 MeV) and 4^+, 6^+, 8^+ (1.44-1.56 MeV) levels in ^{210}Po are well isolated from other expected levels (see Figure 18) and were observed in both (^{12}C, ^{10}Be) and (^{16}O, ^{14}C). The cross sections are given in Table I. The $4\text{-}8^+$ multiplet was not resolved so we consider here the summed cross sections to the individual states.

In Table IV we compare relative cross sections for the 0^+, 2^+ and unresolved $4\text{-}8^+$ levels calculated assuming various wave functions: pure $(1h_{9/2})^2$, KH-I and KH-II[43], and MT.[44] Also included are calculations for ^{210}Po 0^+ g.s. using single particle amplitudes deduced[17] from the proton pick up reaction ^{210}Po (t,α) and assuming constructive phases between amplitudes. The form factor was calculated with the SI method and CK wave functions for ^{12}C and ^{16}O, refs. 39 and 40. We list separately cross sections calculated in the same (arbitrary) units and the ratio calculation/experiment normalized to the $4\text{-}8^+$ cross sections as indicated. The latter procedure would yield a unique DWBA normalization if the $4\text{-}8^+$ levels were pure $(h_{9/2})^2$. The $(h_{9/2}f_{7/2})$ mixtures are important, however, and therefore the DWBA normalization used in Table IV is model dependent to a factor of about 2. We have in several instances used an average normalization based on the $4^+ + 6^+ + 8^+$ calculations for KH-II and MT wave functions (denoted by superscript^h in Table IV). The results obtained with and without corrections for recoil are similar, except for the absolute normalizations (see Appendix).

The calculations presented in Table IV indicate the following:

(1) as expected, the pure $(h_{9/2})^2$ wave functions grossly underestimate the 0^+ g.s. cross sections; (2) the KH-II and MT calculations both overestimate the 0^+ g.s. and 2^+ cross sections by factors 2 to 15; (3) the 0^+ g.s. calculations based on KH-I or the wave functions deduced from $^{210}Po(t,\alpha)$ are in good agreement with the experimental data for (^{12}C, ^{10}Be) but overestimate the (^{16}O, ^{14}C) cross sections.

2. Enhancement of 0^+ g.s. and 2^+ Cross Sections

Yoshida[45] and others[46] have shown that the short range, attractive nuclear forces which lower the energies of the first 0^+, 2^+, 3^-,... states in nuclei introduce correlations which also enhance two-nucleon transfers to these states. Such correlations, of course, are included in "realistic" shell model calculations such as KH and MT. These correlations, e.g., introduce constructive phases for the terms comprising the coherent sum indicated by Eq. (2a), and can result in a large enhancement of the cross sections compared to other transitions.

In the last column of Table IV we list enhancement factors, EF, deduced for the ^{210}Po 0^+ g.s. and 2^+ states as follows: we define EF to be the enhancement in the observed cross section compared to that expected for a pure shell model configuration, in this case $(h_{9/2})^2$. We give values of EF deduced with different DWBA normalizations: the 0^+ g.s. values EF = 3.57 and 1.89 for (^{12}C, ^{10}Be) and (^{16}O, ^{14}C), respectively, have been deduced assuming pure $(h_{9/2})^2$ wave functions for the 4-8^+ multiplet whereas EF = 9.09 and 6.60 have been deduced using an average normalization from KH-II and MT calculations. The latter EF values are presumably more realistic. Using the "realistic" normalizations we conclude that the ^{210}Po 0^+ g.s.

cross section is enhanced (as defined above) by a factor ~ 8 and the 2^+ cross section by a factor ~ 3 in the heavy ion two proton transfer reactions (^{12}C, ^{10}Be) and (^{16}O, ^{14}C).

We may compare the value EF ~ 8 for ^{210}Po g.s. (Z = 84, N = 128) with the enhancement factors deduced by von Oertzen[48] for (^{16}O, ^{14}C) on several nuclei Z $\sim$ 26 to 64 (N $\sim$ 26 to 82). Using the semi-classical transfer probabilities, he obtains[48] (relative to $^{54}Fe(^{16}O, ^{14}C)^{56}Ni$ g.s.[7]) EF ~ 5 for $^{88}Sr(^{16}O, ^{14}C)^{90}Zr$ g.s.[7] and EF ~ 20 for $^{144}Sm(^{16}O, ^{14}C)^{146}Gd$ g.s.[48]. The enhancement factors obtained for the two-proton transfer (^{16}O, ^{14}C) in the region Z $\sim$ 26 to 84 are found to be comparable (when defined in an analogous manner) with those deduced[46] from two neutron transfers, (t,p) and (p,t), within the corresponding neutron shells (i.e., N $\sim$ 26 to 84). This implies that the p-p and n-n correlations are comparable within the same shell.

The enhancement (EF ~ 3) of the 2^+ quadrupole state at 1.18 MeV is comparable to the B(E2) enhancement observed in inelastic scattering from this state[16] ($G_\lambda = 3.5 \pm 1.5$ s.p.u., see Table III). The 3^- octupole state at 2.387 MeV was not observed in the present experiment. Although this state is very collective[16] ($G_\lambda = 46 \pm 15$ s.p.u.) the main two-proton configurations in this state would be $(h_{9/2}\, i_{13/2})_{3^-}$ and $(f_{7/2}\, i_{13/2})_{3^-}$. The former, dominant, configuration is not favored ($0^+ \rightarrow j_< j'_>$, $J \neq j + j'$) while the latter configuration is expected[43,44] to have a small amplitude (< 0.1). Thus, we would not expect this level to be strongly excited in (^{12}C, ^{10}Be) or (^{16}O, ^{14}C) compared to other levels in the energy region $E_x \sim$ 2-3 MeV.

VII. DISCUSSION

Levels in ^{210}Po Observed With (^{12}C, ^{10}Be) and (^{16}O, ^{14}C)

In the following sections we discuss the levels observed in this experiment and suggest their predominant configurations. These suggested "assignments" are based on a comparison with known[13-19] levels in ^{210}Po and energies and cross sections calculated with shell model wave functions[39,40,43,44] (e.g., Figures 16-18), and are therefore very model dependent. The experimental excitation energies are those listed in Table III, unless otherwise noted.

In a preliminary report of this experiment[47], initial calculations indicated that the $(f_{7/2})^2$ and $(f_{7/2}\ f_{5/2})$ configurations would be dominant. The present calculations, however, using "realistic" wave functions, and fewer approximations, give different results, particularly for levels $E_x \sim 4$ MeV.

All levels in ^{210}Po $E_x < 4.98$ MeV are particle stable. The proton, neutron, and alpha separation energies are 4.98, 7.65 and 5.41 MeV, respectively, while the two-proton and two-neutron separation energies are 8.78 and 14.62 MeV, respectively.

A. Levels $E_x < 6.0$ MeV

Below $E_x = 6.0$ MeV, levels seen in both (^{12}C, ^{10}Be) and (^{16}O, ^{14}C) must be due to excitation of ^{210}Po, since the first known excited state in ^{14}C is at $E_x = 6.09$ MeV (see Section III.A). Levels seen only in (^{12}C, ^{10}Be), $E_x > 3.3$ MeV could be due to excitation of either ^{210}Po or ^{10}Be, but as discussed in III.A most groups $E_x < 6$ MeV are believed to be levels in ^{210}Po.

1. $E_x = 0$, 1.19, 1.46 MeV. These levels are well separated from all other expected levels and are therefore assumed to be the 0^+, 2^+ and unresolved $4^+ + 6^+ + 8^+$ (mainly 4^+) levels seen in other work (see Table III).

2. E_x = 2.27 MeV. This group appears to consist of more than one level (see Figure 4 and Table I). Calculations (Figures 18-20) suggest that $(f_{7/2})^2$ 0^+ is the main component although $(f_{7/2}\ h_{9/2})$ 6^+ and 8^+ known to be at 2.188 and 2.336 MeV, respectively, should also be excited particularly in (^{12}C, ^{10}Be). The $(f_{7/2})^2$ 0^+ level is calculated by Ma-True[44] to be at E_x = 2.19 MeV (2.68 MeV KH-II[43]).

3. E_x = 2.56. Calculations indicate that this state is probably the $(h_{9/2}\ f_{7/2})$ 2^+ level [mixed with $(f_{7/2})^2$ 2^+] predicted to be at 2.451 MeV by Ma-True[44] (2.43 MeV KH-II).[43] This is not consistent with (α,t) and (τ,d) work, however, which has all $(h_{9/2}\ f_{7/2})$ strength below 2.43 MeV.[18,19]

4. E_x = 2.85 and 3.05 MeV. These levels are close in energy to known $(h_{9/2}\ i_{13/2})$ levels (11^- and 5-9^-, respectively). Our calculations, however, predict significant strength only to the 9^- state (Figures 18-20). Most of the strength should go to the $(f_{7/2})^2$ 2^+ and $(f_{7/2})^2$ 4^+ and 6^+ levels. The former is calculated by Ma-True to be at 2.65 MeV (2.97 MeV KH-II) while the latter are at 3.10 and 3.28 MeV (3.24 and 3.31 MeV, KH-II). Also, the relative cross sections seen in (^{12}C, ^{10}Be) and (^{16}O, ^{14}C) indicate small L transfers. This is consistent with these states being 2^+ and 4^+ (+ 6^+) rather than 11^- and 9^-.

5. E_x = 3.41 MeV. A group is seen in (^{12}C, ^{10}Be) at this energy but is absent (or very weak) in (^{16}O, ^{14}C). This group is consistent with a transition to ^{210}Po (g.s.) and $^{10}Be^*$ (2^+), the latter being at 3.37 MeV. The width of this group, however, appears to be narrow compared to that expected from broadening[3] due to γ-decay in flight (300-400 keV). An alternate possibility is that this level is the $(f_{7/2})^2$ 6^+ state in ^{210}Po, but this is not

very consistent with the calculations, particularly the expected $4^+ - 6^+$ splitting (see Figures 18-20). There is a level seen in $^{210}Po(p,p')$ with weak intensity at 3.437 MeV. This latter data would be most consistent with this being the $(f_{7/2}\ i_{13/2})\ 3^-$ state, however, calculations place this state at 3.70 MeV.

6. E_x = 3.70 and 4.07 MeV. The calculations favor these states being mainly the $(f_{7/2}\ i_{13/2})\ 3^-$ and 5^- levels predicted by Ma-True[44] to be at 3.69 and 3.94 MeV, respectively (3.62 and 3.93 Mev, KH-II).[43] The level at 3.70 MeV, however, is populated more strongly in (^{12}C, ^{10}Be) than expected for the 3^- level, and would be more consistent with a higher spin value (e.g., $(f_{7/2})^2\ 6^+$). Although there have been several negative parity and/or collective states seen in this region (Table III) all are unassigned or assigned $J \geq 4$.

7. E_x = 4.36 and 4.53 MeV. These groups appear to be most consistent with their being composed of members of the $(h_{9/2}\ p_{3/2})$ multiplet seen[18,19] in (α,t) and (τ,d). The 4.53 MeV group is likely to be the $(h_{9/2}\ p_{3/2})\ 6^+$ level predicted by Ma-True[44] to be at this energy (4.52 Mev, KH-II).[43]

There are several isomeric states in this region seen[14,15] in $(\alpha, 2n\gamma)$. These states, however, involve core excitation which is not believed to be an important mechanism in the (^{12}C, ^{10}Be) and (^{16}O, ^{14}C) reactions (see Section IV.).

8. E_x = 4.95 and 5.07 MeV. The 4.95 and 5.07 MeV levels [unresolved in (^{16}O, ^{14}C)] are calculated to be mainly $(f_{7/2}\ p_{3/2})\ 2^+$ and 4^+ predicted by Ma-True[44] to be at 5.13 and 5.33 MeV (5.22 and 5.50 MeV, KH-II).[43] Excitation of the 16^+ isomeric state at 5.058 MeV[14,15] would not be likely since core excitation would be required. Also, L = 16 is not particularly favored kinematically (see Figures 10 and 11).

9. E_x = 5.33, 5.53, and 5.81 MeV. Groups are observed at these energies with both (^{12}C, ^{10}Be) and (^{16}O, ^{14}C) although it is not clear that the same groups are excited in these reactions (see Table I). The group seen in (^{12}C, ^{10}Be) at E_x = 5.53 is much stronger than any groups observed in (^{16}O, ^{14}C) near this energy (see Figures 18-20). Also, there are no states predicted to be populated as strongly as is observed. This suggests two possibilities: the group at 5.53 MeV is due to $^{10}Be^*$ (3.37 MeV) and $^{210}Po^*$ (2.27 MeV), or it is an excited state of ^{210}Po not included in the shell model basis considered here[43,44], e.g., a state from the next oscillator shell. If the latter be the case, its structure and spin must be such that it would be preferentially populated in (^{12}C, ^{10}Be), e.g. $(j_<)^2$ and large J, respectively.

B. E_x > 6 MeV

Above 6 MeV excitation many groups appear in either or both the (^{12}C, ^{10}Be) and (^{16}O, ^{14}C) spectra (see Table I). Any "assignments", however, are limited by the fact that the groups observed may be due to projectile excitation. A broad structure seen in (^{16}O, ^{14}C) $E_x \sim 7$ MeV appears (Figure 3) to be due to $^{14}C^*$. The angular distribution to a part of this structure (E_x = 7.25 MeV) is different from others (see Figure 7), although the measurements contain considerable uncertainties due to background subtraction.

A level $E_x \sim 6.06$ MeV appears in both (^{12}C, ^{10}Be) and (^{16}O, ^{14}C) and is probably a level in ^{210}Po. Furthermore, identifiable peaks are observed in several (^{16}O, ^{14}C) spectra at $E_x \sim$ 8.7, 9.4, 10.0, 10.7, 11.7, and 12.3 MeV (see Table I). The relatively narrow widths of these peaks (see Figure 3) suggest that they are levels in ^{210}Po, although above E_x = 8.78 MeV the two-proton configurations in ^{210}Po are unbound.

VIII. CONCLUSIONS

We may summarize the results presented above as follows:

(i) The two-proton transfer reactions $^{208}Pb(^{12}C, ^{10}Be)^{210}Po$ and $^{208}Pb(^{16}O, ^{14}C)^{210}Po$ selectively populate many previously unobserved levels in ^{210}Po.

(ii) The measured angular distributions show no reliable L or J signature, which precludes model-independent assignments.

(iii) The theoretical calculations, however, exhibit features which are sensitive to the structure and spin of the projectile and target states and indicate that the levels observed are predominantly the $(2f_{7/2})^2$ 0^+, 2^+, 4^+, 6^+, $(2f_{7/2}\ 1i_{13/2})$ 3^-, 5^-, and $(2f_{7/2}\ 3p_{3/2})$ 2^+, 4^+ states predicted by shell model calculations.

(iv) The cross sections to the 0^+ (g.s.) and 2^+ (1.18 MeV) levels in ^{210}Po are found to be enhanced by factors ~ 8 and ~ 3, respectively, compared to those expected for pure $(h_{9/2})^2$ configurations. Calculations using "realistic" projectile and target shell model wave functions, however, overestimate the 0^+ (g.s.) and 2^+ cross sections by factors of 2 to 15.

(v) The gross features of the observed spectra, $E_x \lesssim 7$ MeV, are reproduced by the calculations, and in particular the differences in the $(^{16}O, ^{14}C)$ and $(^{12}C, ^{10}Be)$ spectra.

IX. ACKNOWLEDGEMENTS

We thank the staff and crew of the 88" cyclotron for providing us with the necessary ^{16}O and ^{12}C beams, C. Ellsworth for preparing the targets, and Björn Nilsson, L. Jardine and M. A. Nagarajan for discussion and advice. We also thank Professor William True for supplying shell model wave functions and R. DeVries for providing a copy of the finite-range DWBA program LOLA.

APPENDIX

1. CMI Form Factor

In this section we present details of the c. m. interaction (CMI) method of calculating the DWBA form factor for heavy ion two-nucleon transfers, specifically (^{16}O,^{14}C) and (^{12}C,^{10}Be). The method is based on the Moshinsky-Talmi expansion[31] as described in Refs. 25 and 26 with some simplifications which facilitate the calculations.

DWBA requires the evaluation of the six dimensional integral[23,24]

$$T = \int d^3\underset{\sim}{r}\ \chi_f^{(-)*}(\underset{\sim}{k}_f,\underset{\sim}{r}_f)\ \langle Bb|V|Aa\rangle\ \chi_i^{(+)}(\underset{\sim}{k}_i,\underset{\sim}{r}_i) \tag{A1}$$

for the reaction A(a,b)B. The coordinate system for two-nucleon transfer (B = A + 2, a = b + 2) is shown in Fig. 21. If the mass transfer is small compared with the masses (m_a,m_B) of a or B, then (A1) can be reduced to three dimensional integrals through use of the no-recoil approximations[23,24]

$$\underset{\sim}{r}_i(=\underset{\sim}{r}_{aA}) = \underset{\sim}{r}_{bA} + \frac{2}{m_a}\underset{\sim}{R}_1 \tag{A2a}$$

$$\doteq \underset{\sim}{r}_{bA} \tag{A2b}$$

$$\underset{\sim}{r}_f(= -\underset{\sim}{r}_{Bb}) = \frac{m_A}{m_B}\underset{\sim}{r}_{bA} - \frac{2}{m_B}\underset{\sim}{R}_1 \tag{A2c}$$

$$\doteq \frac{m_A}{m_B}\underset{\sim}{r}_{bA} \tag{A2d}$$

In some calculations, the use of the no-recoil approximation can introduce large errors.[21,22] We have investigated these effects and discuss them in Sec. 3.

If the no-recoil approximations (A2b) and (A2d) are used, the total form factor $\langle Bb|V|Aa \rangle$ can be written as

$$\langle Bb|V|Aa \rangle = \sum_{J_1 J_2 L} C_{J_1 J_2 L}(R) F_{J_1 J_2 L}(R)\, Y^*_{LM}(\hat{R}) \tag{A3}$$

where $C_{J_1 J_2 L}$ is a coupling coefficient and $\underset{\sim}{R} = \underset{\sim}{r}_{bA}$.

The radial form factor, $F_{J_1 J_2 L}(R)$, for two-nucleon transfer is obtained by expanding the motion of the transferred nucleon pair into relative and center of mass (c.m.) motion (see Fig. 21). The nucleon p(p') is in the shell model orbit $n_1 \ell_1 j_1$ $(n_1' \ell_1' j_1')$ in the nucleus "a" and in the state $n_2 \ell_2 j_2$ $(n_2' \ell_2' j_2')$ in "B". The c.m. radial wave functions of the di-nucleon cluster relative to cores A and b are denoted by $U_{N_2 \Lambda_2}(R_2)$ and $U_{N_1 \Lambda_1}(R_1)$, respectively. The motion of p relative to p' in a and B is given by $u_{\tilde{n}_1 \tilde{\ell}_1}(\tilde{r}/2)$ and $u_{\tilde{n}_2 \tilde{\ell}_2}(\tilde{r}/2)$, respectively. The transferred nucleons are coupled to $J = J_1$ in nucleus a and $J = J_2$ in nucleus B. The total spins of A, B, a and b are J_A, J_B, J_a and J_b, respectively. The quantity L is the orbital angular momentum transfer between A and B. We consider the transfer of two identical nucleons and assume that the effective interaction is spin-independent and acts only the c.m. of transferred nucleon pair. It can be shown that[25,26]

$$F_{J_1J_2L}(R) = (-1)^{J_1-J_2+L+1} \sqrt{4\pi}\, \hat{J}_2 \sum_{\substack{L_1S_1\\N_1\Lambda_1}} \sum_{\substack{\tilde{n}_1\tilde{\ell}_1\\\tilde{n}_2\tilde{\ell}_2}} \sum_{\substack{L_2S_2\\N_2\Lambda_2}} \Omega_{12}$$

$$\times\, G^{\tilde{n}_1\tilde{\ell}_1}_{N_1\Lambda_1}(L_1S_1J_1)\; G^{\tilde{n}_2\tilde{\ell}_2}_{N_2\Lambda_2}(L_2S_2J_2)(-1)^{\Lambda_1-\Lambda_2}\hat{\Lambda}_1\hat{\Lambda}_2\; \hat{L}_1\hat{L}_2\; \delta_{S_1S_2}\; \delta_{\tilde{\ell}_1\tilde{\ell}_2} \qquad \text{(A4)}$$

$$\times\, (\Lambda_1 0\Lambda_2 0|L0)\; W(L_1L_2\Lambda_1\Lambda_2, L\tilde{\ell}_1)\; W(L_1L_2J_1J_2, LS_1)\; U_L^{12}(R)$$

where

$$\hat{J} \equiv (2J+1)^{1/2}$$

$$\Omega_{12} = 4\pi \int dr\, r^2\, u_{\tilde{n}_1\tilde{\ell}_1}(r)\, u_{\tilde{n}_2\tilde{\ell}_2}(r)$$

$$\leqslant 1$$

and

$u_{n\ell}(r)$ = harmonic oscillator function (size parameter ν).

The structure factor G is similar to that defined by Glendenning[25] for (p,t), etc., and is given by

$$G^{\tilde{n}_1\tilde{\ell}_1}_{N_1\Lambda_1}(L_1S_1J_1) = \sum_{\substack{n_1\ell_1j_1\\ n_1'\ell_1'j_1'}} g\, B(n_1\ell_1j_1n_1'\ell_1'j_1'J_aJ_bJ_1)$$

$$\times \langle (\tfrac{1}{2}\,\ell_1)j_1\ (\tfrac{1}{2}\,\ell_1')j_1'J_1 | (\ell_1\ell_1')L_1S_1J_1 \rangle \tag{A5}$$

$$\times \langle \tilde{n}_1\tilde{\ell}_1N_1\Lambda_1L_1 | n_1\ell_1n_1'\ell_1'L_1 \rangle \quad .$$

The last two factors in (A5) are a jj to LS coupling coefficient and a Moshinsky-Talmi bracket,[31,49] respectively. If the nuclear wave functions have definite symmetry then[25] $g = 1/\sqrt{2}$ if $n_1\ell_1j_1 = n_1'\ell_1'j_1'$, otherwise $g = 1$. The factor $B\ (n_1 \cdots)$ in A5 is the two-nucleon coefficient of fractional parentage (c.f.p.):$\langle a | \} b \rangle$. The structure factor $G^{\tilde{n}_2\tilde{\ell}_2}_{N_2\Lambda_2}(L_2S_2J_2)$ is defined in a manner analogous to (A5).

The quantum numbers N_1, Λ_1, $\tilde{n}_1$, $\tilde{\ell}_1$ etc. allowed in the sum (A5) are constrained to satisfy the conditions[31,49]

$$2N_1 + \Lambda_1 + 2\tilde{n}_1 + \tilde{\ell}_1 = 2n_1 + \ell_1 + 2n_1' + \ell_1' \tag{A6a}$$

and

$$2N_2 + \Lambda_2 + 2\tilde{n}_2 + \tilde{\ell}_2 = 2n_2 + \ell_2 + 2n_2' + \ell_2'$$

with

$$\tilde{\ell}_1 = \tilde{\ell}_2 \tag{A6b}$$

and

$$|\Lambda_1 - \Lambda_2| \leqslant L \leqslant \Lambda_1 + \Lambda_2$$

We note, however, that (A6a) and (A6b) allow $\tilde{n}_2 \neq \tilde{n}_1$.

The function $U_L^{12}(R)$ in (A4) is the overlap of the di-nucleon cluster wave functions $U_{N_1\Lambda_1}(R_1)$ and $U_{N_2\Lambda_2}(R_2)$ projected onto R. Buttle and Goldfarb[5] and Sawaguri and Tobocman,[50] among others, have developed methods for calculating such functions.

One finds that for reactions between strongly absorbed projectiles, such as ^{12}C and ^{16}O on heavy nuclei, the functions $U_L^{12}(R)$ need only be calculated at large R (see Sec. V). This can be readily done with the Buttle and Goldfarb (BG) addition theorem.[5] The function $U_{N_2\Lambda_2}(R_2)$ is approximated asymptotically by a Hankel function

$$U_{N_2\Lambda_2}(R_2) \longrightarrow N_{N_2\Lambda_2}\, h_{\Lambda_2}^{(1)}(i\kappa_2 R_2) \tag{A7a}$$

and then[5]

$$U_L^{12}(R) \longrightarrow N_{N_2\Lambda_2}\, A_{N_1\Lambda_1}\, h_L^{*(1)}(i\kappa_2 R) \tag{A7b}$$

where

$$A_{N_1\Lambda_1} = \int_0^\infty dr\, r^2\, j^*_{\Lambda_1}(i\kappa_2 r)\, V_{cm}(r)\, U_{N_1\Lambda_1}(r) \quad . \tag{A7c}$$

The potential $V_{cm}(r)$ is the effective interaction acting on the c.m. of the transferred nucleons. In the calculations described here, $V_{cm}(r)$ was chosen to be a Woods-Saxon potential which binds the di-nucleon system in the projectile (post representation).

If $U_{N\Lambda}(r)$ describes a di-neutron then $\kappa = (2m_{2n}\ B_{2n}/\hbar^2)^{1/2}$ where m_{2n} is the di-neutron mass and B_{2n} is its separation energy. Proton transfers can be treated using the integral expansion given in Ref. 26. Instead, we calculate proton transfers by replacing κ_2 with an effective value, $\bar{\kappa}$ ($> \kappa_2$) obtained by fitting a Hankel function to $U_{N_2\Lambda_2}(R_2)$ in a region spanning the interaction radius ($R \approx R_m \doteq 12$ fm). This procedure is found to work quite well for single proton transfers.[20] Although κ varies slightly with N_2 and Λ_2 one can, with suitable renormalization, use a value common to all N_2 and Λ_2, so that the form factor can be factorized

$$F_{J_1J_2L}(R) = f^{12}_{J_1J_2L}\, h_L^{*(1)}\ (i\bar{\kappa}R) \tag{A8a}$$

We may, further, replace $h_L^{*(1)}$ $(i\bar{\kappa}R)$ by $h_0^{*(1)}$ $(i\kappa R)$ $(= e^{-\kappa R}/\kappa R)$ so that

$$F_{J_1J_2L}(R) \doteq f_0\ h_0^{*(1)}\ (i\kappa R) \tag{A8b}$$

where f_0 and κ are obtained by matching (A8b) to (A8a) in the region $R \doteq R_m$ (see Fig. 13).

The cross sections for the stripping reactions (^{16}O,^{14}C g.s.) and (^{12}C,^{10}Be g.s.) i.e. $J_a = J_b = 0$ on target nuclei $J_A = 0$ are then given by

$$\frac{d\sigma}{d\Omega} = |f_0|^2\ \sigma_L^{DW}\ (\theta,\kappa) \tag{A9}$$

with $J_1 = 0$ and $L = J_2 = J_B$. The quantity, σ_L^{DW} (θ,κ) is the DWBA cross section (including $2L + 1$) calculated with the form factor $h_0^{*(1)}$ $(i\kappa R)$. The nuclear

structure information is included in the factor $|f_0|^2$ while σ_L^{DW} (θ,κ) contains the reaction dynamics. In a limited region of excitation it is often most useful to fix κ and instead renormalize only f_0 in order to account for binding energy effects. This allows one to extrapolate cross sections from calculated Q-windows such as Figs. 10 and 11 rather than perform numerous and lengthy individual calculations. Equations (A8b) and (A9) are also convenient in that analytic expressions for σ_L^{DW} (θ,κ) may often be used, particularly below the Coulomb barrier.[32-34] Configuration mixing is easily included in the structure factor f_0, without recalculation of σ_L^{DW} (θ,κ).

Since the CMI form factor (A8b) diverges at small radii it is necessary to introduce a cut-off in the DWBA radial integrals. In Fig. 22 we show the dependence of the DWBA peak cross sections versus cut-off radius R'_{CO} for $^{208}Pb(^{12}C,^{10}Be)$, Q = -20 and -28 MeV. The calculations converge for $R_{CO} \lesssim 9.5$ fm. This can be attributed to the strong absorption of the distorted waves for R < 10 fm, resulting in localization of the reaction in ℓ- and R-space as discussed in Sec. V (Figs. 12 and 13).

Calculations[51] have been performed for $^{208}Pb(^{12}C,^{10}Be)^{210}Po$ and $^{208}Pb(^{16}O,^{14}C)^{210}Po$ using the CMI method and approximations (A7) and (A8b). The clusters $U_{N\Lambda}(R)$ in the projectile and target are bound in Woods-Saxon wells ($R = 1.28\ A^{1/3}$ fm, a = 0.76 fm) at the appropriate two-proton separation energies, fit with Hankel functions and the sum indicated in (A4) performed. Typical values of terms in A4-A7 are given in Ref. 26. The coefficients $N_{N_1\Lambda_1}$, $N_{N_2\Lambda_2}$, and $A_{N_1\Lambda_1}$ are analoguous to the coefficients $N_{n_1\ell_1}$, $N_{n_2\ell_2}$ and $A_{n_1\Lambda_2}$ required for single nucleon transfer[5] and exhibit the same properties

e.g. $N_{N_2\Lambda_2}$ increases rapidly with N_2 and less rapidly with Λ_2 while $A_{N_1\Lambda_1} \propto N_{N_1\Lambda_1} (\kappa_2)^{\Lambda_1}/(\kappa_1)^{(\Lambda_1+1)}$. Also $\Omega_{12} \approx 0.9$ for $\tilde{n}_1 = \tilde{n}_2$ and decreases rapidly for $\tilde{n}_2 \neq \tilde{n}_1$.

A comparison of the terms in (A4) indicates that for the ^{12}C and ^{16}O wave functions used here[39,40] (intermediate coupling) the target configurations with the largest $\tilde{n}\tilde{\ell}$ = 1S components are favored. Next in importance are $\tilde{n}\tilde{\ell}$ = 2S and finally $\tilde{n}\tilde{\ell}$ = 1P. The latter terms are important if jj-coupled projectile wave functions are considered, since the jj to LS transformation (A5) introduces terms whose signs depend on whether $j_2(j_2') = \ell_2(\ell_2') + \frac{1}{2}$ or $\ell_2(\ell_2') - \frac{1}{2}$ i.e., $j_>j_>'$, $j_<j_<'$ or $j_<j_>'$, $j_>j_<'$ (see e.g. Ref. 26) There is also a J-dependence within a multiplet $(j_2j_2')_J$ (Eqs. 6a, 6b Sec. V-E) which depends on the jj to LS transformation properties and the amount of relative 1S motion contained in the configuration $(j_2j_2')_J$.

2. Numerical Results

In Fig. 23 we compare (^{12}C,^{10}Be) asymptotic form factors for the dominant configurations in ^{210}Po calculated with the CMI and SI methods. The CMI and SI calculations shown differ as follows: the CMI method treats the effective interaction V in (A7c) as a spin-independent potential acting on a di-nucleon cluster bound in the projectile at the two nucleon separation energy while the SI method uses the sum interaction $V = V_1 + V_1'$ where V_1 and V_1' (which include a spin-orbit interaction) bind the individual nucleons in the projectile. Despite these intrinsic differences, the two calculations give qualitatively the same features: 1) the p^2, f^2 and fp single nucleon

configurations are favored; 2) two classes of transitions are observed $0^+ \rightarrow j_> j'_>$ of $j_< j'_<$ (type I) and $0^+ \rightarrow j_> j'_<$ or $j_< j'_>$ (type II); and 3) at least for (^{12}C,^{10}Be), $0^+ \rightarrow j_>^2$ is favored over $0^+ \rightarrow j_<^2$.

There are, however, quantitative differences (factor $\gtrsim 2$ in $|F(R)|^2$) which are largest for unfavored transitions i.e. those with poor relative S-state components. The $0^+ \rightarrow (1h_{9/2})^2$ and $0^+ \rightarrow (1i_{13/2})^2$ transitions, for example, are factors of 50 to 100 times weaker in the CMI calculations than in the SI method. Also, there appears to be differences in relative form factors for spin orbit partners e.g. $p_{3/2}^2 - p_{1/2}^2$, $f_{7/2}^2 - f_{5/2}^2$, etc.

The systematics of the CMI calculations shown in Fig. 23 are very similar to those one would deduce for (^3He,n) from the appropriate structure factors.[41] In (^3He,n) or (p,t) one would have $|f_0|^2$ for 0^+ states $(3p_{3/2})^2$: $(3p_{1/2})^2$: $(2f_{7/2})^2$: $(2f_{5/2})^2$: approximately the ratios 1:0.5:0.4:0.3 compared to 1:0.41:0.16:0.15 calculated for (^{12}C,^{10}Be). The (^3He,n) and (^{12}C,^{10}Be) cross sections, of course, depend on the behaviour of σ_L^{DW} (θ). If, however, Eq. 4 (Sec. V) would also apply to (^3He,n) i.e. if this reaction were localized in R-space similar to (^{12}C,^{10}Be), then one would expect 0^+ cross sections in proportion to the $|f_0|^2$ values noted above (provided the levels were nearly degenerate, i.e. had the same Q-value).

The close similarity between (^{12}C,^{10}Be) and (^3He,n) structure factors arises from the large 1S relative di-proton component contained in the ^{12}C wave functions of Cohen-Kurath.[39,40] (^{16}O,^{14}C) would be expected to be more dissimilar since the ^{16}O wave functions are closer to jj-coupling (see Fig. 15). Only in the limits of pure jj-coupling projectile wave functions are large

(>>2) differences expected (see Fig. 15). The usefulness and (apparently) accuracy of the CMI method is determined to a large degree by the extent to which the relative 1S and 2S di-nucleon components are important in the projectile and target. We have not, however, attempted to reconcile in detail the differences in the CMI and SI results.

Detailed investigations of these methods as applied to two neutron transfers, mainly (^{18}O,^{16}O), may be found in the refs. 26,28-30. Some of the features discussed above for (^{12}C,^{10}Be) and (^{16}O,^{14}C) have also been noted for two-neutron transfer reactions.[26,28-30]

3. Recoil Effects

One of the uncertainties associated with DWBA analyses of heavy-ion induced transfer reactions concerns the effect of the recoil terms [Eqs. (A2a-d)] neglected in the usual DWBA calculations.[20-22] Recoil terms have been found to be important in single-nucleon transfers, where both the DWBA amplitudes and allowed L values are affected.[11,20-22]

We have estimated the effects of recoil for the two-proton transfer (^{16}O, ^{14}C) and (^{12}C, ^{10}Be) in the following manner: the two nucleons are assumed to be transferred as a cluster with relative motion $\tilde{n}_1\tilde{\ell}_1 = \tilde{n}_2\tilde{\ell}_2 = 1S$ and singlet spin. Since $J_1=J_a=J_b=J_A=0$ only $L=J_2=J_B$ is allowed and from (A6), $\Lambda_1 = 0$ and $\Lambda_2 = L$. The term with $\tilde{n}_1\tilde{\ell}_1 = \tilde{n}_2\tilde{\ell}_2 = 1S$ and $L = \Lambda_2$ is usually the most important one in the sum (A4).

The di-proton clusters were bound in the projectile and target in Woods-Saxon potentials with $R = 1.28A^{1/3}$ fm, a = 0.76 fm and V adjusted to fit the two-proton separation energies.

No-recoil DWBA calculations were performed with finite-range form factors generated using the Sawaguri-Tobocman method[50,52] and the DWBA amplitudes were evaluated in a no-recoil DWBA program.[23] Calculations including recoil were then made using the same di-proton wave functions but with a non-local form factor and DWBA amplitudes determined with an exact finite-range DWBA program.[52] The differences between the two sets of calculations represent an estimate of the effect of recoil in the evaluation of the DWBA amplitudes.

Calculations have been performed for L = 0, 2 and 6 for (^{16}O, ^{14}C), Q = -13.6, -18.6 and -24.6 MeV and (^{12}C, ^{10}Be), Q = -18.6 and -24.6 MeV. The results are presented in Table V. The following features are observed: (1) the relative cross sections for different L-values (≤ 6) at the same Q-value are not substantially altered by recoil; (2) the Q-dependence of the cross sections, i.e., the Q-windows (Figures 10 and 11) are affected, however, with recoil introducing a shift in Q_{opt} of ~ -4 MeV; (3) the position of the maxima in the angular distributions calculated with and without recoil are similar and shift with Q value whereas the data do not (see Figures 6, 7 and 14); and (4) the absolute DWBA normalization changes with the inclusion of recoil. Features similar to (2) and (4) have been noted by Buttle and Goldfarb[20] and DeVries and Kubo[22] in their analyses of single nucleon transfers.

The recoil effects indicated in Table V can be simulated by application of emperically determined correction factors to the no-recoil DWBA cross sections, i.e.,

$$\sigma_L^{DW}\ (\text{recoil}) \doteq \mathcal{N}_1 f(Q)\sigma_L^{DW}\ (\text{no recoil}) \qquad \text{(A10a)}$$

where

$$f(Q) = \exp(-0.162Q) \qquad \text{(A10b)}$$

with

$$\mathcal{N}_1 = 0.25 \text{ for } (^{16}O,\ ^{14}C)$$
$$= 0.30 \text{ for } (^{12}C,\ ^{10}Be) \quad . \qquad \text{(A10c)}$$

Eqs. (A10a-c) were determined from calculations $L \leq 6$ and -24 MeV $\leq Q \leq -13$ MeV but may also be valid outside these limits. Alternate procedures to the one suggested above could also be derived from the recoil approximations given by Buttle and Goldfarb[20] or Nagarajan.[21]

The results noted above indicate that recoil corrections should be included in DWBA analyses of data spanning a range of several MeV in Q value. Thus we have included the correction (A10a-c) in the calculation of the (^{12}C, ^{10}Be) and (^{16}O, ^{14}C) spectra (Figures 19 and 20). The recoil correction reduces the calculated 0^+ g.s. cross sections by a factor ~ 2 compared with those to the strong 2^+ state at $E_x \sim 5$ MeV. The enhancement factors (Table IV), however, do not depend sensitively on the recoil correction since all the calculations are for $Q \approx Q$ g.s.

FOOTNOTES AND REFERENCES

*Work performed under the auspices of the U.S. Atomic Energy Commission.

†Present address: Cyclotron Laboratory, Physics Department, University of Michigan, Ann Arbor, Michigan 48105.

‡Present address: Argonne National Laboratory, Argonne, Illinois.

‡Permanent address: Hahn-Meitner Institute, Berlin, Germany.

1. R. E. Hintz, F. B. Selph, W. S. Flood, B. G. Harvey, F. G. Resmini, and E. A. McClatchie, Nucl. Instr. Methods 72, 61 (1969).

2. B. G. Harvey, J. Mahoney, F. G. Pühlhofer, F. S. Goulding, D. A. Landis, J. C. Faivre, D. G. Kovar, M. S. Zisman, J. R. Meriwether, S. W. Cosper, and D. L. Hendrie, Nucl. Instr. Methods 104, 21 (1972).

3. M. S. Zisman, F. D. Becchetti, B. G. Harvey, D. G. Kovar, J. Mahoney, and J. Sherman, Phys. Rev. C (in press).

4. B. G. Harvey, H. Homeyer, J. Mahoney and G. Gabor, 1972 LBL Progress Report, LBL-1666, p. 366 (unpublished).

5. P. J. A. Buttle and L. J. B. Goldfarb, Nucl. Phys. 78, 409 (1966).

6. J. Phys. 32, supp. 11-12 (1971); R. J. Nickles et al., Phys. Rev. Letters 26, 1267 (1971); Proc. of Heavy Ion Summer Study (ORNL CONF-7200669, 1972); K. Nagatani, M. Ichimura, and A. Arima, Physica Scripta 6, 289 (1972).

7. P. R. Christensen, V. I. Manko, F. D. Becchetti, and R. J. Nickles, Nucl. Phys. A207, 33 (1973).

8. T. Lauritzen and F. Ajzenberg-Selove, Nucl. Phys. 78, 1 (1966); D. E. Alburger, et al., Phys. Rev. 85, 1242 (1969).

9. Taken from compilation of F. Ajzenberg-Selove, Nucl. Phys. A152, 1 (1970).

10. M. Conjeaud, S. Harar, and C. Volant, Proc. of E.P.S., Aix-en-Provence. 2, II.40 (1972).

11. D. G. Kovar, F. D. Becchetti, B. G. Harvey, F. G. Pühlhofer, J. Mahoney, D. W. Miller, and M. S. Zisman, Phys. Rev. Letters 29, 1023 (1972); D. G. Kovar et al., Phys. Rev. Letters 30, 1075 (1973).

12. J. S. Larsen, J. L. C. Ford, Jr., R. M. Gaedke, K. S. Toth, J. B. Ball, and R. L. Hahn, Phys. Letters 42B, 205 (1972).

13. L. J. Jardine and S. G. Prussin, Nucl. Phys. A190, 261 (1972).

14. T. Yamazaki, Phys. Rev. C1, 290 (1970); I. Bergström, B. Fant, and K. Wilström, Physica Scripta 3, 103 (1971).

15. B. Fant, Physica Scripta 4, 175 (1971).

16. C. Ellegaard, P. D. Barnes, R. Eisenstein, E. Romberg, T. S. Bhatia, and T. R. Canada, Nucl. Phys. A206, 83 (1973).

17. P. D. Barnes, E. Romberg, C. Ellegaard, R. F. Casten, Ole Hansen, T. J. Mulligan, R. Broglia, and R. Liotta, Nucl. Phys. A195, 146 (1972).

18. R. Tickle and J. Bardwick, Phys. Letters 36B, 32 (1971).

19. W. A. Lanford, W. P. Alford, and H. W. Fulbright, preprint.

20. P. J. A. Buttle and L. J. B. Goldfarb, Nucl. Phys. A176, 299 (1971).

21. M. A. Nagarajan, Nucl. Phys. A196, 34 (1972).

22. R. M. DeVries and K. I. Kubo, Phys. Rev. Letters 30, 325 (1973).

23. P. D. Kunz, University of Colorado reports COO-535-606 and COO-535-613 (unpublished).

24. N. Austern, Direct Nuclear Reactions Theories (Wiley Interscience, New York, 1972), chap. 5.

25. N. K. Glendenning, Phys. Rev. 137, B102 (1965).

26. R. Broglia, T. Kammuri, R. Liotta, A. Winther, and B. Nilsson, J. Phys. 32, Suppl. 11-12, C6-151 (1971); R. Broglia, R. Liotta, A. Winther, B. Nilsson, and T. Kammuri, preprint.

27. R. Ascuitto and N. K. Glendenning, Nucl. Phys. A188, 185 (1972).

28. A. J. Baltz and S. Kahana, Phys. Rev. Letters 29, 1267 (1972).

29. R. Ascuitto and N. K. Glendenning, (unpublished).

30. A. Roberts, Nucl. Phys. A196, 465 (1973).

31. I. Talmi, Helv. Phys. Acta 25, 185 (1952); M. Moshinsky, Nucl. Phys. 13, 104 (1959).

32. D. Trautmann and K. Alder, Helv. Phys. Acta 43, 363 (1970); K. Alder and D. Trautmann, Nucl. Phys. A178, 60 (1971).

33. A. Winther, J. Phys. 32, Suppl. 11-12, C6-83 (1971); R. Broglia and A. Winther, Phys. Reports 4C, 153 (1972).

34. K. Alder, R. Morf, M. Pauli, and D. Trautmann, Nucl. Phys. A191, 399 (1972).

35. D. Kovar, Proc. of ANL Heavy Ion Symposium (ANL, 1973); LBL-1654, (unpublished).

36. F. D. Becchetti, P. R. Christensen, V. I. Manko, and R. J. Nickles, Phys. Letters 43B, 279 (1973).

37. H. J. Körner, G. C. Morrison, L. R. Greenwood, and R. H. Seimssen, Phys. Rev. C7, 107 (1973).

38. J. V. Maher, K. A. Erb, and R. W. Miller, Phys. Rev. C7, 651 (1973).

39. S. Cohen and D. Kurath, Nucl. Phys. A101, 1 (1967).

40. S. Cohen and D. Kurath, Nucl. Phys. A141, 145 (1970).

41. N. K. Glendenning, Tables of Structure Amplitudes for (p,t) Reactions, UCRL-18268 (1968), (unpublished).

42. Y. E. Kim and J. O. Rasmussen, Nucl. Phys. 47, 184 (1963); Nucl. Phys. 61, 173 (1965).

43. G. H. Herling and T. T. S. Kuo, Nucl. Phys. A181, 113 (1972); T. T. S. Kuo and G. H. Herling, NRL Memorandum Report 2258 (1971).

44. C. W. Ma and W. W. True, submitted to Phys. Rev. C; W. W. True, private communication.

45. S. Yoshida, Nucl. Phys. 33, 685 (1962).

46. N. K. Glendenning, Phys. Rev. 156, 1344 (1966); invited paper, Washington APS Meeting 1968 (UCRL 18225, unpublished).

47. F. D. Becchetti et al., B.A.P.S. 18, 714 (1973); 1972 LBL progress report, LBL-1666, p. 95, (unpublished).

48. W. von Oertzen, H. G. Bohlen, and B. Gebauer, Nucl. Phys. A207, 91 (1973).

49. T. A. Brody and M. Moshinsky, Tables of Transformation Brackets (Gordon and Breach, New York, 1967).

50. T. Sawaguri and W. Tobocman, J. Math. Phys. 8, 2223 (1967).

51. Program HITN, F. D. Becchetti (unpublished); (Moshinsky-bracket routine written by M. S. Zisman).

52. Program RDRC, W. Tobocman (unpublished).

53. Program LOLA, R. DeVries (unpublished).

Table I. Groups Observed in This Experiment

$^{208}Pb(^{12}C, ^{10}Be)^{210}Po$ E_L = 78 MeV		$^{208}Pb(^{16}O, ^{14}C)^{210}Po$ E_L = 104 MeV		$^{208}Pb(^{16}O, ^{14}C)^{210}Po$ E_L = 140 MeV	
E_x [a] (MeV)	$\int\sigma$ [b] (μb)	E_x [c] (MeV)	$\int\sigma$ [d] (μb)	E_x [e] (MeV)	$\sigma(37.5°)$ (μb/sr)
0	94 ± 15	0	47 ± 15	0	16 ± 4
1.19	36 ± 9	1.14	23 ± 10	0.75	9 ± 3
1.46 [g]	46 ± 11 [g]	1.47	37 ± 14	1.42	31 ± 6
2.27 [g]	300 ± 30 [g]	2.32	205 ± 30	2.29	65 ± 7
2.56	55 ± 8	2.51	41 ± 13 [f]	—	—
2.85	214 ± 21	2.84	247 ± 31 [f]	3.01	108 ± 11
3.05 [g]	291 ± 29 [g]	3.08	182 ± 20 [f]	—	—
3.41 [g,h]	83 ± 19 [g,h]	—	—	—	—
3.70	394 ± 31	3.70	281 ± 32 [f]	3.74	104 ± 11
4.07 [g]	247 ± 24 [g]	4.06	217 ± 31 [f]	4.12	68 ± 7
4.36	41 ± 8	—	—	—	—
4.53	70 ± 11	4.50	91 ± 27	—	—
4.95	366 ± 29	—	—	—	—
5.07	122 ± 17	5.03 [g]	682 ± 79 [g]	4.95	128 ± 8
5.33 [g]	199 ± 23 [g]	—	—	5.27	60 ± 6
5.53 [h]	450 ± 36 [h]	5.43 [g]	289 ± 34 [g]	—	—
5.81	82 ± 15	5.68	189 ± 34	5.71	149 ± 15
6.06	173 ± 20	6.04	203 ± 25	—	—
6.29	66 ± 16	6.29	200 ± 25	—	—
6.49	60 ± 9	—	—	—	—

(continued)

Table I. (continued)

$^{208}Pb(^{12}C, ^{10}Be)^{210}Po$ E_L = 78 MeV		$^{208}Pb(^{16}O, ^{14}C)^{210}Po$ E_L = 104 MeV		$^{208}Pb(^{16}O, ^{14}C)^{210}Po$ E_L = 140 MeV	
E_x a) (MeV)	$\int\sigma$ b) (μb)	E_x c) (MeV)	$\int\sigma$ d) (μb)	E_x e) (MeV)	$\sigma(37.5°)$ (μb/sr)
6.76 g)	96 ± 15 g)	6.71	250 ± 30	—	—
—	—	6.93 h)	311 ± 34 h)	6.84 h)	159 ± 15 h)
7.38	96 ± 17	7.25 h)	357 ± 36 h)	—	—
7.75 g)	182 ± 26 g)	7.66	336 ± 35	7.63	169 ± 16
8.1	—	—	—	—	—
—	—	8.71	384 ± 38	8.77	183 ± 18
—	—	9.44	393 ± 39	9.23	93 ± 14
—	—	9.95	265 ± 27	10.02	209 ± 20
—	—	10.26	256 ± 27	—	—
—	—	10.66	504 ± 50	10.81	386 ± 25
—	—	11.02	289 ± 29	—	—
—	—	11.40	386 ± 39	—	—
—	—	11.70	—	11.66	341 ± 25
—	—	12.30	—	12.17	291 ± 20

a) ±30 keV, E_x < 6 MeV; ±50 keV, E_x > 6 MeV

b) Integrated cross section θ = 44° to 82° (c.m.). Statistical errors are given.

c) ±40 keV, E_x < 6 MeV; ±60 keV, E_x > 6 MeV

d) Integrated cross section θ = 33° to 79° (c.m.) except as noted. Statistical errors are given.

e) ±60 keV

f) Integrated θ = 40° to 79° (c.m.).

g) Unresolved group of states.

h) May be due to projectile excitation (see Section VI).

Table II. Comparison of Spectroscopic Factors for ^{210}Po and ^{209}Bi

Reaction	E_x [a] (MeV)	$d\sigma/d\Omega$ (mb/sr)	Assumed s.p. [b]	Ratio [c] $C^2S(^{210}Po)/C^2S(^{209}Bi)$
$^{209}Bi(^{12}C, ^{11}B)^{210}Po$	1.18	0.16 ± 0.04	$1h_{9/2}$	0.73 ± 0.08
E_L = 78 MeV	1.52	1.10 ± 0.11		
θ_L = 65°	2.37	1.92 ± 0.14	$2f_{7/2}$	0.70 ± 0.06
	2.94	0.44 ± 0.07	$1i_{13/2}$	0.89 ± 0.10
	3.20	0.65 ± 0.08		
	4-5.8	2.12 ± 0.21	$2f_{5/2}$ - 3p	1.03 ± 0.11
$^{209}Bi(^{16}O, ^{15}N)^{210}Po$	1.55	0.25 ± 0.02	$1h_{9/2}$	0.92 ± 0.09
E_L = 104 MeV	2.40	2.64 ± 0.08	$2f_{7/2}$	0.95 ± 0.04
θ_L = 67.5°	3.11	0.79 ± 0.04	$1i_{13/2}$	0.90 ± 0.04
	4-5.8	3.33 ± 0.13	$2f_{5/2}$ - 3p	1.14 ± 0.04

a) Excitation energy of centroid (±50 keV). See Figure 8.

b) States in ^{210}Po assumed to be multiplets formed by coupling single particle configuration listed to ^{209}Bi ($1h_{9/2}$) g.s.

c) Ratio of summed spectroscopic factors for levels in ^{210}Po and ^{209}Bi as deduced from cross section ratios using ^{209}Bi data from reference 11.

Table III. Levels in ^{210}Po

Previous Work				This Work	
E_x a) (MeV)	J^{π} b)	G_{λ} c) (s.p.u.)	$[J_f/J_i]C^2S$ d)	E_x e) (MeV)	J^{π} f)
0	0^+		0.18	0	(0^+)
1.181	2^+	3.5 ± 1.5	1.05	1.19	(2^+)
1.437	4^+	(weak)	1.82		
1.473	6^+		2.65	1.46	$(4^+ + 6^+ + 8^+)$
1.556	8^+		3.30		
2.188	8^+		1.91		
—	—	—	—	2.27	$(0^+ + 8^+)$
2.290	$(2^+, 3^+)$	(weak)	0.47		
2.336	6^+		1.40		
2.382	4^+		(1.1)		
2.387	3^-	46 ± 15			
2.403	5^+		(1.3)		
2.405	(1^+)				
2.413	3^+		(0.7)		
2.438	7^+		(1.6)		
—	—	—	—	2.56	(2^+)
2.658 c)		(weak)			
2.849	11^-		3.10		
—	—	—	—	2.85	(2^+)
2.874 c)		(weak)			
2.910	5^-	13 ± 4	0.54		
2.999	(9^-)		(1.6)		
3.009	(2^-)				
3.017	7^-		(3.2)		
3.026	5^-	16 ± 5			
—	—	—	—	3.05	(4^+)
3.075	4^-		0.75		
3.111	(3^-)				
3.125	6^-		(1.2)		

(continued)

Table III. (continued)

Previous Work				This Work	
E_x [a] (MeV)	J^{π} [b]	G_{λ} [c] (s.p.u.)	$[J_f/J_i]C^2S$ [d]	E_x [e] (MeV)	J^{π} [f]
3.138	(8^-)		(1.8)		
3.183	10^-		2.33		
3.428	(4^-)				
3.437 [c]		(weak)		3.41 [h]	
3.525	$(5,6)^-$				
3.699	$(4^{\pm},5^{\pm},6^{\pm})$				
—	—	—	—	3.70	(3^-)
3.711	$(4^{\pm},5^{\pm},6^{\pm})$				
3.727	$(5)^-$				
3.780	$(4^-,5^-,6^-)$		~ 0.5		
3.801 [c]		(weak)			
4.032 [d]		(weak)	~ 1		
4.105 [c]		(weak)		4.07	(5^-)
4.142 [d]		(weak)	~ 2		
4.237 [c]		(weak)			
4.336 [d]			~ 0.5		
4.324 [g]	11^-				
4.346 [c]		(weak)			
4.372 [g]	13^-				
4.377 [d]		(weak)	~ 1	4.36	
4.466 [d]			~ 1		
4.542 [d]			~ 2.5	4.53	(6^+)
4.636 [d]			~ 4		
4.666 [d]					
4.777 [g]	13^-				
4.948 [d]			~ 0.5		
—	—	—	—	4.95	(2^+)
—	—	—	—	5.07	(4^+)

(continued)

Table III. (continued)

Previous Work				This Work	
E_x a) (MeV)	J^π b)	G_λ c) (s.p.u.)	$[J_f/J_i]C^2S$ d)	E_x e) (MeV)	J^π f)
5.058 g)	16^+				
5.151 d)			weak		
5.223 d)			~ 0.5		
—	—	—	—	5.33	
				5.53 h)	
				5.81	
				6.06	
				6.29	
				6.49	
				6.76	
				6.93 h)	
				7.38	
				7.75	
				(See Table I)	

a) Excitation in ^{210}Po taken from compilation of data given in reference 13, except as noted. Errors typically < ±3 keV.

b) Taken from compilation reference 13 except as noted.

c) (p,p') results (reference 16). Errors in E_x ±10 keV.

d) References 18 and 19.

e) Results from (^{12}C, ^{10}Be) except as noted. Errors ±30 keV, E_x < 6 MeV ± 50 keV, E_x > 6 MeV (see also Table I and Figure 18).

f) The spins listed are suggested assignments based on shell model predictions and calculated transition strengths (see Section VI and Figure 18). The data, however, do not contain unambiguous spin signatures which permit direct spin assignments.

g) (α,2nγ) results (references 14 and 15).

h) May be due to projectile excitation (see Section VI).

Table IV. Comparison of Experimental and Calculated Cross Sections to the $(h_{9/2})^2$ Multiplet in ^{210}Po

	E_x a) (MeV)	J^π	w.f. ^{210}Po b)		$\int\sigma$ c) (μb)	Calculated Cross Section d) (arb.)	calc./exp. e)	EF f)
(^{12}C, ^{10}Be) 78 MeV:	0	0^+	pure	$h^2_{9/2}$	94 ± 15	0.146	0.28	3.57
			—		—	—	—	9.09 h)
			MT			3.0	2.09	
			KH-II			3.58	3.30	
			KH-I			1.75	1.23 h)	
			(t,α) g)			1.30	0.92 h)	
	1.19	2^+	pure	$h^2_{9/2}$	36 ± 9	1.35	0.67	1.49
			—		—	—	—	3.79 h)
			MT			1.52	2.77	
			KH-II			0.64	1.51	
	1.46	$4\text{-}8^+$	pure	$h^2_{9/2}$	46 ± 11	0.26	1.0 e)	
			MT			0.70	1.0 e)	
			KH-II			0.54	1.0 e)	
(^{16}O, ^{14}C) 104 MeV:	0	0^+	pure	$h^2_{9/2}$	47 ± 15	0.10	0.53	1.89
			—		—	—	—	6.60 h)
			MT			6.41	8.67	
			KH-II			7.60	14.50	
			KH-I			3.49	5.52 h)	
			(t,α) g)			2.45	3.86 h)	
	1.14	2^+	pure	$h^2_{9/2}$	23 ± 10	1.08	1.25	0.80
			—		—	—	—	2.80 h)
			MT			3.34	9.36	
			KH-II			1.23	4.89	
	1.47	$4\text{-}8^+$	pure	$h^2_{9/2}$	37 ± 14	0.14	1.0 e)	
			MT			0.58	1.0 e)	
			KH-II			0.41	1.0 e)	

(continued)

Table IV. (continued)

a) From Table I ($\leqslant \pm 40$ keV).

b) Wave functions used for ^{210}Po: MT (reference 44), KH-II (reference 43, approximation 2), KH-I (reference 43, approximation 1), (t,α) (reference 17). Cohen-Kurath wave functions used for ^{16}O and ^{12}C (reference 40, set a).

c) From Table I ($\theta \sim 40° - 80°$ c.m.).

d) DWBA calculation using V_{SI} form factor (see text).

e) Ratio theory/experiment normalized to calculated sum of 4^+, 6^+ and 8^+ levels for wave functions noted, except for KH-I and (t,α) (see footnote h).

f) Enhancement of cross section as deduced from ratio of experiment to theory using DWBA normalization to 4^+, 6^+ and 8^+ states assuming pure $(h_{9/2})^2$ or mixed wave functions for the latter (see footnote h).

g) Using single-particle amplitudes deduced from an ^{210}Po(t,α) experiment (reference 17) and constructive phases.

h) Using an average of the normalization for the 4^+, 6^+ and 8^+ states obtained with MT and KH-II wave functions.

Table V. Comparison of Exact and No-recoil DWBA Calculations

Reaction	Q (MeV)	E_x (MeV)	L	Exact DWBA[a] $\theta^{d)}_{peak}$ (deg.)	Exact DWBA[a] $\sigma_L^{DW}(\theta)^{e)}$ (μb/sr)	No-recoil DWBA[b] $\theta^{d)}_{peak}$ (deg.)	No-recoil DWBA[b] $\sigma_L^{DW}(\theta)^{e)}$ (μb/sr)	Ratio[c] Exact / No-recoil
$^{208}Pb(^{12}C,^{10}Be)$	-18.6	0	0	63	35.2	63	5.2	6.8
E_L = 78 MeV			2	62	141.5	63	21.1	6.7
			6	62	80.6	63	12.1	6.7
	-24.6	6	0	89	5.9	82	0.40	14.8
			2	80	29.6	80	1.91	15.5
			6	73	43.4	73	2.63	16.5
$^{208}Pb(^{16}O,^{14}C)$	-13.6	0	0	62	47.4	62	21.1	2.24
E_L = 104 MeV			2	62	170.5	62	76.3	2.23
			6	62	61.8	63	27.9	2.21
	-18.6	5	0	65	40.0	67	7.6	5.25
			2	65	166.5	67	31.5	5.28
			6	65	105.8	65	19.9	5.32
	-24.6	11	0	78	5.21	80	0.42	12.4
			2	77	28.1	78	2.16	13.0
			6	72	48.9	73	3.51	13.9

a) Exact finite-range DWBA calculation (ref. 53) assuming a di-proton transfer with $\tilde{n}_1\tilde{\ell}_1 = \tilde{n}_2\tilde{\ell}_2 = 1S$ and $\Lambda_2 = L$ (see text). Optical parameters (Woods-Saxon): V = -40 MeV, W = -15 MeV, R = 1.31 $(A_1^{1/3} + A_2^{1/3})$ fm and a = 0.45 fm.

b) Same as exact DWBA calculation (a) above except no-recoil approximation Eq. (A4) is used (refs. 23, 50 and 52).

c) Ratio of peak cross sections for exact and no-recoil DWBA calculations (see footnotes (a) and (b)).

d) Calculated position (c.m.) of maximum in the differential cross section.

e) The maximum value of the DWBA differential cross section (i.e., $\theta = \theta_{peak}$). These values do not include the spectroscopic amplitudes for the projectile or target (see text).

FIGURE CAPTIONS

Fig. 1. Schematic diagram of experimental apparatus. Top: Spectrometer. Bottom: Electronics for focal plane counter. The dashed curves represent particle trajectories.

Fig. 2. An energy loss ($\Delta E/\Delta X$) vs. time-of-flight (T.O.F.) spectrum at the spectrometer field setting (Fig. 3) for $^{14}C(6^+)$. $\Delta E/\Delta X$ and T.O.F. have been corrected for dependence on $B\rho$ (reference 2). m/q (top) is the approximate mass to charge ratio for the groups indicated:

a: $^{16}O(7^+)$, b: $^{17}O(7^+)$, c: $^{18}O(7^+)$,
d: $^{15}N(7^+)$, e: $^{15}N(6^+)$, f: $^{13}C(6^+)$,
g: $^{14}C(6^+)$, h: $^{12}C(5^+)$, i: $^{13}C(5^+)$

Fig. 3. A position spectrum (summed over six wires) for $^{14}C(6^+)$ (thick target), E_L = 104 MeV. Excitation energies are given in Table I.

Fig. 4. Top: A comparison of (^{16}O, ^{14}C) and (^{12}C, ^{10}Be) spectra (thin target) near the grazing angle. The energy scales have been adjusted to be approximately the same. Bottom: Excitation energies and spectroscopic factors for ^{210}Po levels $[1h_{9/2} \otimes n\ell j]_J$ observed in $^{209}Bi(\alpha,t)$ and $^{209}Bi(^3He,d)$, references 18 and 19.

Fig. 5. A $^{14}C(6^+)$ spectrum, $E_L(^{16}O)$ = 140 MeV.

Fig. 6. Angular distributions for groups observed in $^{208}Pb(^{12}C, ^{10}Be)$. The smooth curves are no-recoil DWBA calculations (see Section VI.D). The data points have been connected to guide the eye.

Fig. 7. Angular distributions for groups observed in $^{208}Pb(^{16}O, ^{14}C)$. The smooth curves are no-recoil DWBA calculations (see Section VI.D). The data points have been connected to guide the eye.

Fig. 8. Top: Spectra (near the grazing angle) for the single proton transfers (^{16}O, ^{15}N) and (^{12}C, ^{11}B) on ^{209}Bi. Bottom: Position and spectroscopic factors for levels in ^{210}Po observed in $^{209}Bi(\alpha,t)$ and $^{209}Bi(^{3}He,d)$, references 18 and 19.

Fig. 9. The square of the form factor ($MeV^2 fm^{-6}$) calculated (V_{SI} method) for various $0^+ \rightarrow 0^+$ (^{12}C, ^{10}Be) transitions with Cohen-Kurath wave functions for ^{12}C (references 39 and 40, set a) and pure configurations for ^{210}Po. R_m is the radius used in Eq. (4) and is near the interaction radius deduced from the radial integrals (Fig. 13).

Fig. 10. The calculated dependence of no-recoil DWBA peak cross sections on L transfer and excitation energy for (^{12}C, ^{10}Be) using a fixed form factor ($e^{-\kappa R}/\kappa R$, $\kappa = 1.6\ fm^{-1}$).

Fig. 11. The calculated dependence of no-recoil DWBA peak cross sections on L transfer and excitation energy for (^{16}O, ^{14}C) using a fixed form factor ($e^{-\kappa R}/\kappa R$, $\kappa = 1.6\ fm^{-1}$).

Fig. 12. The square of the scattering matrix elements β_L^M (references 23 and 24) vs. ℓ, the total orbital angular momentum in the incident channel. The value of ℓ deduced from the calculated grazing angle assuming pure Coulombic orbits is indicated ($= \ell_{gr}^{c\ell}$). L=M=0 for the g.s. transition.

Fig. 13. The square of the integrand (averaged over 0.5 fm in R) for the radial integral determining β_L^M, $\ell = 37\hbar$ (see Fig. 12).

Fig. 14. Experimental (●) and calculated (V_{CMI} method) peak angle in $d\sigma/d\Omega$ for $^{208}Pb(^{16}O, ^{14}C)$, $E_L = 104$ MeV and $^{208}Pb(^{12}C, ^{10}Be)$, $E_L = 78$ MeV. The calculation shown is for L = 4 (see Figs. 6 and 7).

Fig. 15. Dependence of $|F_L(R_m)|^2$, R_m = 12 fm (see Section V) vs. the projectile configuration: $\alpha\, p^2_{3/2} + \beta\, p^2_{1/2}$ $(\alpha^2 + \beta^2 = 1)$ for 0^+ levels in ^{210}Po of the form $(n\ell j)^2$. Solid curves: $j = j_> = \ell + \frac{1}{2}$, dashed curve: $j = j_< = \ell - \frac{1}{2}$. At the top mixing ratios for various projectile wave functions are indicated: pure $1p^2_{3/2}$; pure $1p^2_{1/2}$; pure LS(^{1}S); and Cohen-Kurath ^{12}C and ^{16}O (references 39 and 40, set a). V_{SI} method used.

Fig. 16. The calculated peak cross sections (V_{SI} method, Eq. (4), no-recoil DWBA) for ^{208}Pb(^{12}C, ^{10}Be) to levels in ^{210}Po of the form $[n\ell j \otimes n'\ell' j']_J$. The j values are denoted by $j_>(\equiv \ell + \frac{1}{2})$ and $j_<(\equiv \ell - \frac{1}{2})$. Solid curves: positive parity; dashed curves: negative parity. Cohen-Kurath wave functions used for ^{12}C (references 39 and 40, set a).

Fig. 17. The calculated peak cross sections (V_{SI} method, Eq. (4), no-recoil DWBA) for ^{208}Pb(^{16}O, ^{14}C) to levels in ^{210}Po of the form $[n\ell j \otimes n'\ell' j']_J$. The j values are denoted by $j_>(\equiv \ell + \frac{1}{2})$ and $j_<(\equiv \ell - \frac{1}{2})$. Solid curves: positive parity; dashed curves: negative parity. Cohen-Kurath wave functions used for ^{16}O (references 30 and 40, set a).

Fig. 18. A comparison of previously known (references 13-19) and predicted (references 43 and 44) levels in ^{210}Po with groups observed in this experiment. The bar graphs represent integrated cross sections (see Table I). Groups labeled "a" could be due to projectile excitation (see Section VI). Suggested level assignments (see text) are indicated by connecting lines: —— positive parity; --- negative parity .

Fig. 19. Observed (top) and calculated (bottom) spectra for (^{12}C, ^{10}Be). The calculations (V_{SI} method, Eq. (4)) use CK (references 39 and 40) and MT (reference 44) wave functions and have been arbitrarily normalized. Corrections for recoil have been included in the DWBA calculations (see text).

Fig. 20. Observed (top) and calculated (bottom) spectra for (^{16}O, ^{14}C). The calculations (V_{SI} method, Eq. (4)) use CK (references 39 and 40) and MT (reference 44) wave functions and have been arbitrarily normalized. Corrections for recoil have been included in the DWBA calculations (see text).

Fig. 21. Coordinate system used in V_{CMI} method.

Fig. 22. Variation of calculated peak cross section vs. radial cut-off in the DWBA integrals.

Fig. 23. Comparison of asymptotic form factors (arbitrary units) calculated for (^{12}C, ^{10}Be) (CK wave functions, references 39 and 40) with (top) V_{CMI} method and (bottom) V_{SI} method. Levels in ^{210}Po of the form $[n\ell j \otimes n'\ell'j']_J$ are considered with j denoted by $j_<(\equiv \ell - \frac{1}{2})$ and $j_>(\equiv \ell + \frac{1}{2})$. Solid curves: positive parity; dashed curves: negative parity.

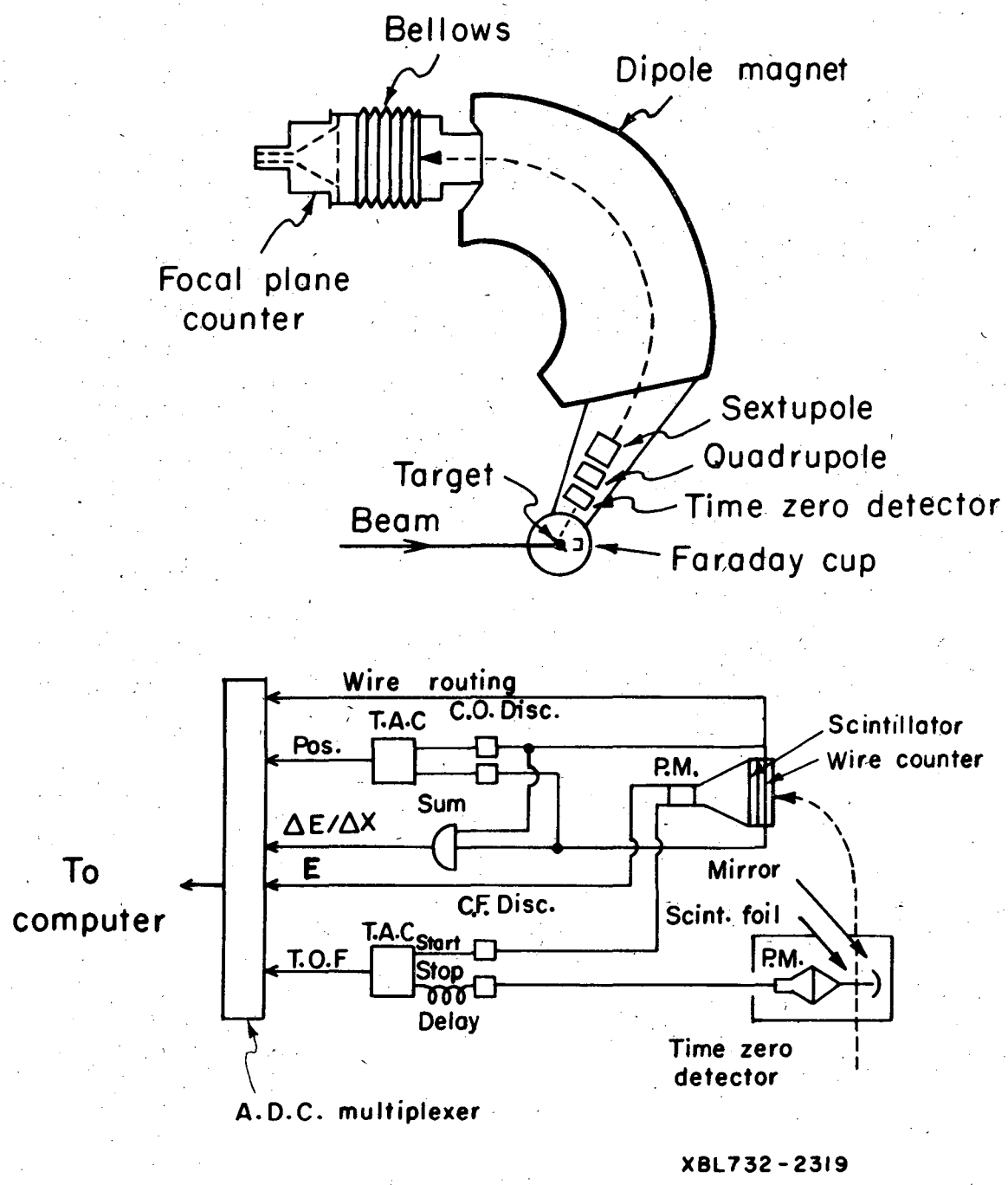
Bellows
Dipole magnet
Focal plane counter
Sextupole
Quadrupole
Target
Time zero detector
Beam
Faraday cup
Wire routing
T.A.C
C.O. Disc.
Scintillator
Wire counter
Pos.
P.M.
Sum
ΔE/ΔX
E
Mirror
To computer
C.F. Disc.
Scint. foil
T.A.C
Start
T.O.F
Stop
P.M.
Delay
Time zero detector
A.D.C. multiplexer
XBL732-2319

Fig. 1

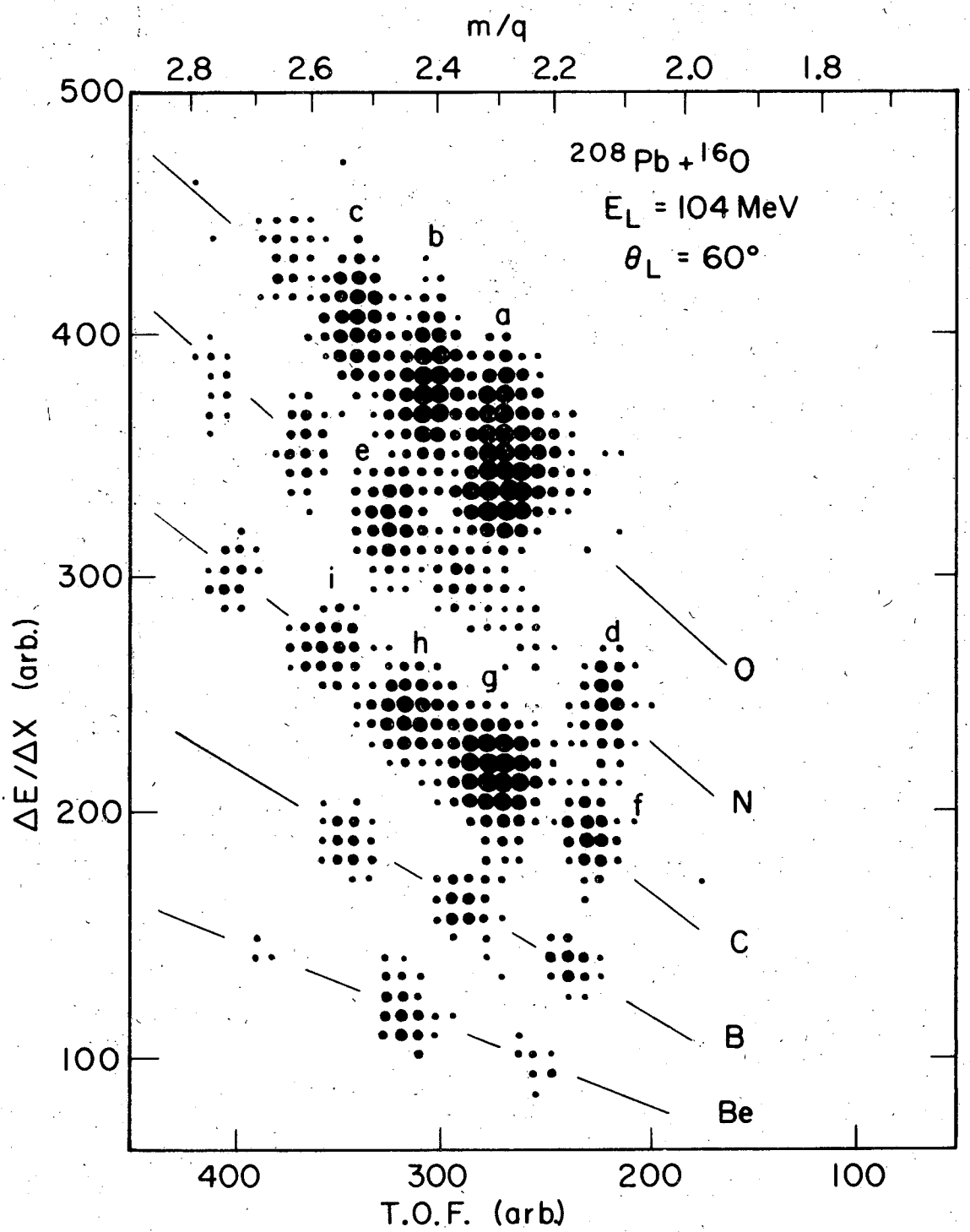

XBL731-2173

Fig. 2

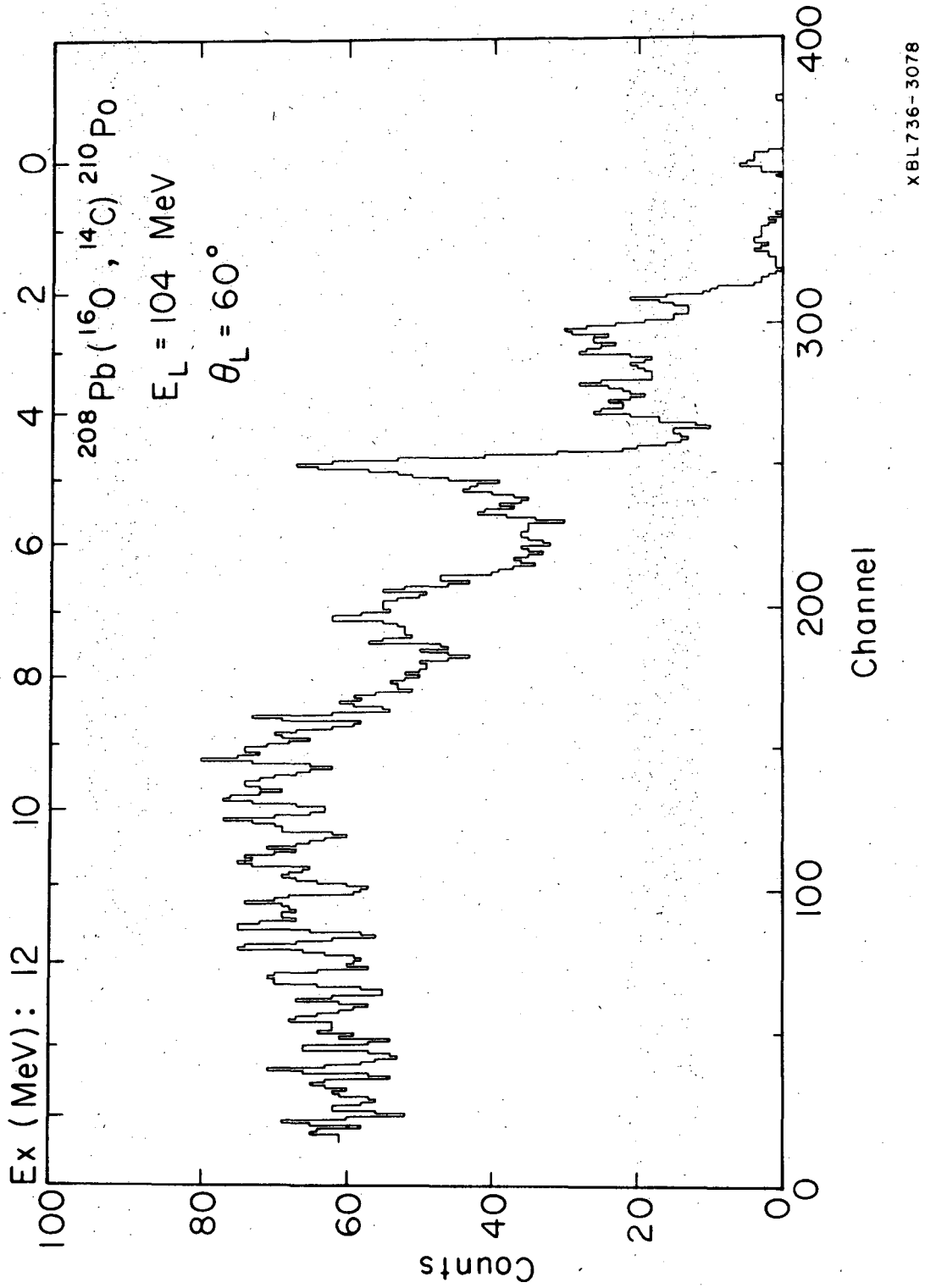
$^{208}Pb(^{16}O, ^{14}C)^{210}Po$
$E_L = 104$ MeV
$\theta_L = 60°$
Ex (MeV): 12 10 8 6 4 2 0
Counts
100 80 60 40 20 0
Channel
0 100 200 300 400
XBL736-3078

Fig. 3

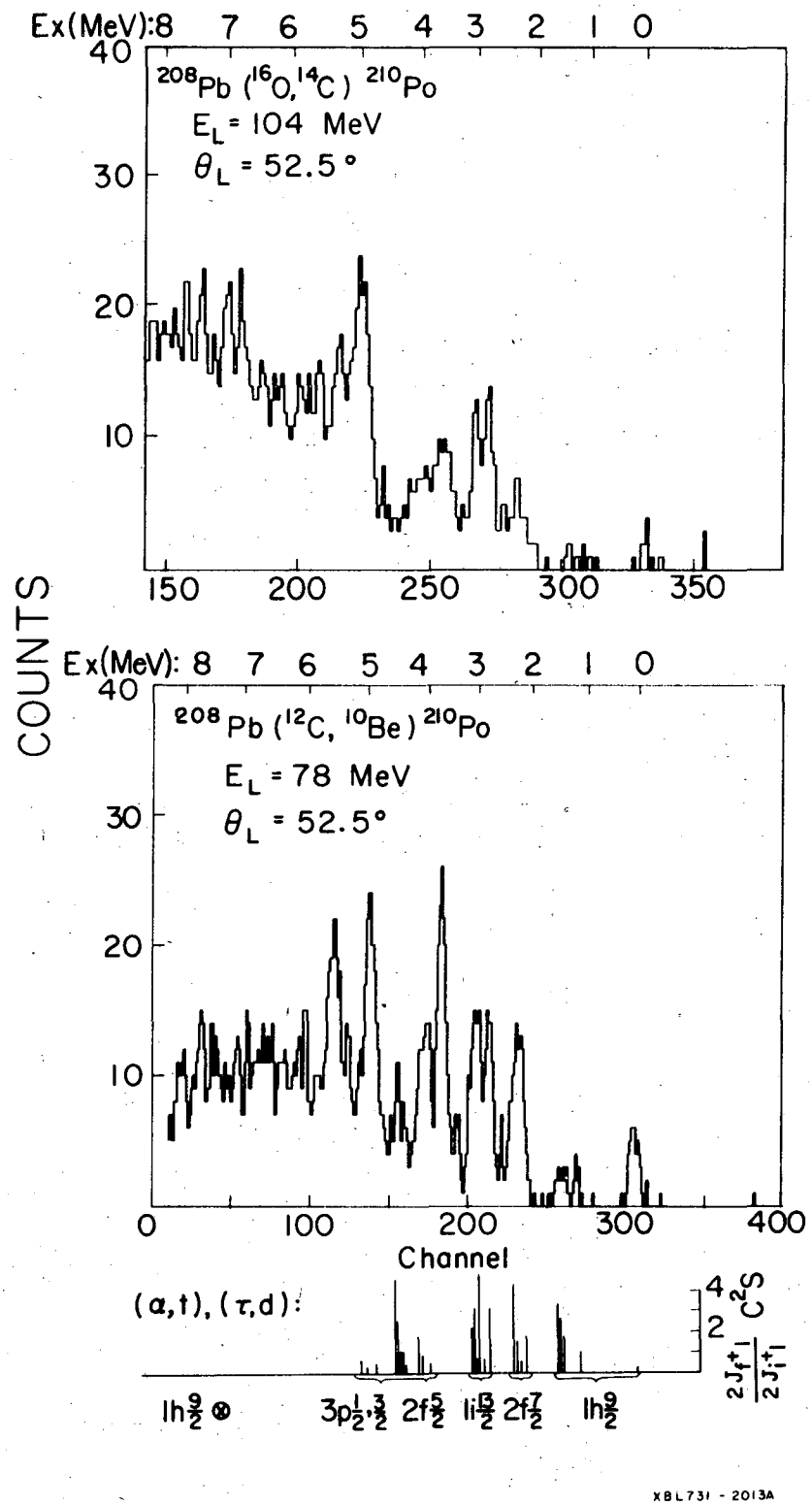
Ex(MeV):8 7 6 5 4 3 2 1 0
^{208}Pb (^{16}O,^{14}C) ^{210}Po
E_L = 104 MeV
θ_L = 52.5°
COUNTS
Ex(MeV): 8 7 6 5 4 3 2 1 0
^{208}Pb (^{12}C, ^{10}Be) ^{210}Po
E_L = 78 MeV
θ_L = 52.5°
Channel
(α,t), (τ,d):
C^2S
$\frac{2J_f+1}{2J_i+1}$
$1h\frac{9}{2}$ ⊗
$3p\frac{1}{2},\frac{3}{2}$ $2f\frac{5}{2}$ $1i\frac{13}{2}$ $2f\frac{7}{2}$ $1h\frac{9}{2}$
XBL731 - 2013A

Fig. 4

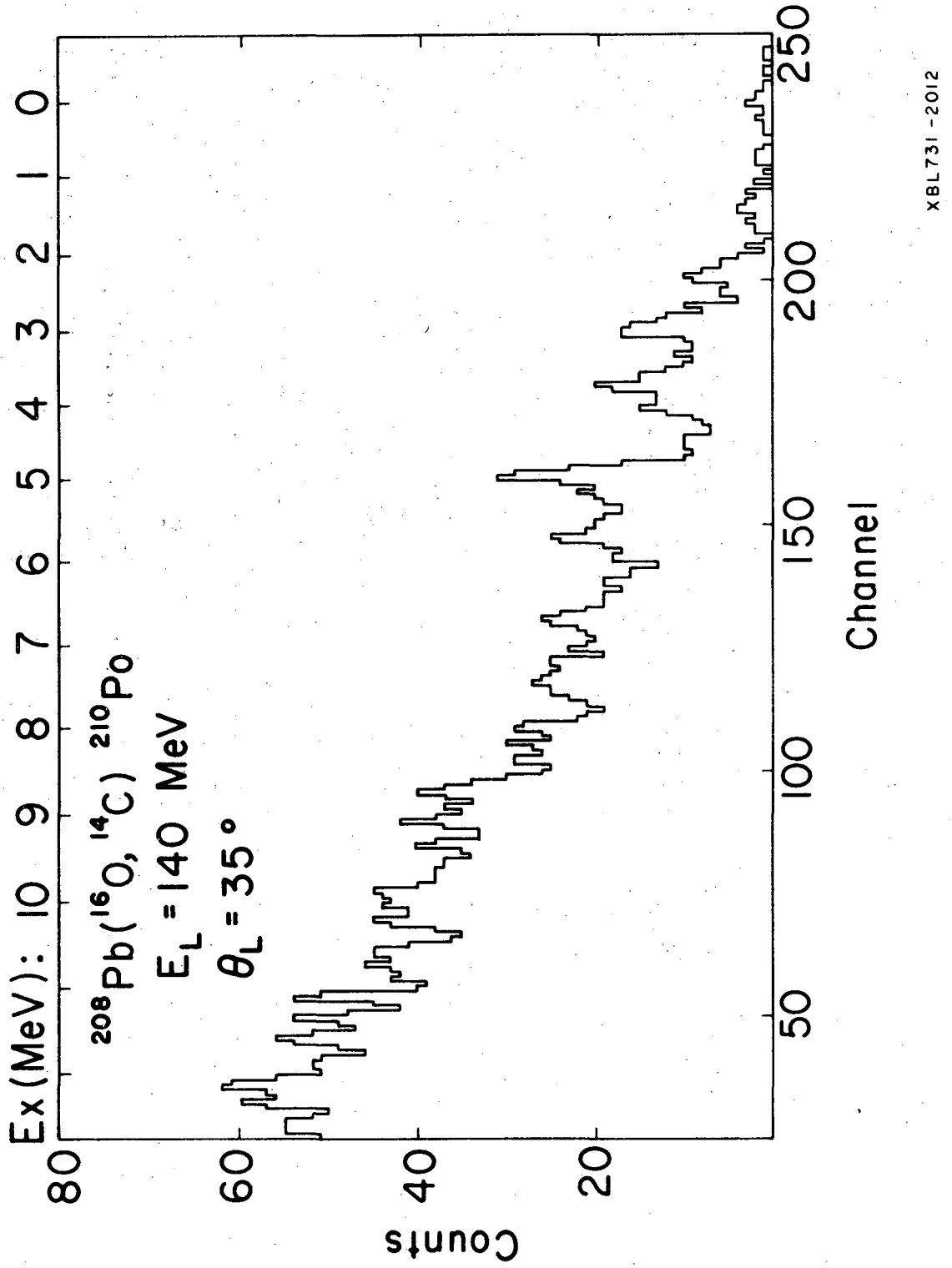
Ex (MeV): 10 9 8 7 6 5 4 3 2 1 0
$^{208}Pb(^{16}O, ^{14}C)\ ^{210}Po$
$E_L = 140$ MeV
$\theta_L = 35°$
Counts
80
60
40
20
Channel
50
100
150
200
250
XBL731-2012

Fig. 5

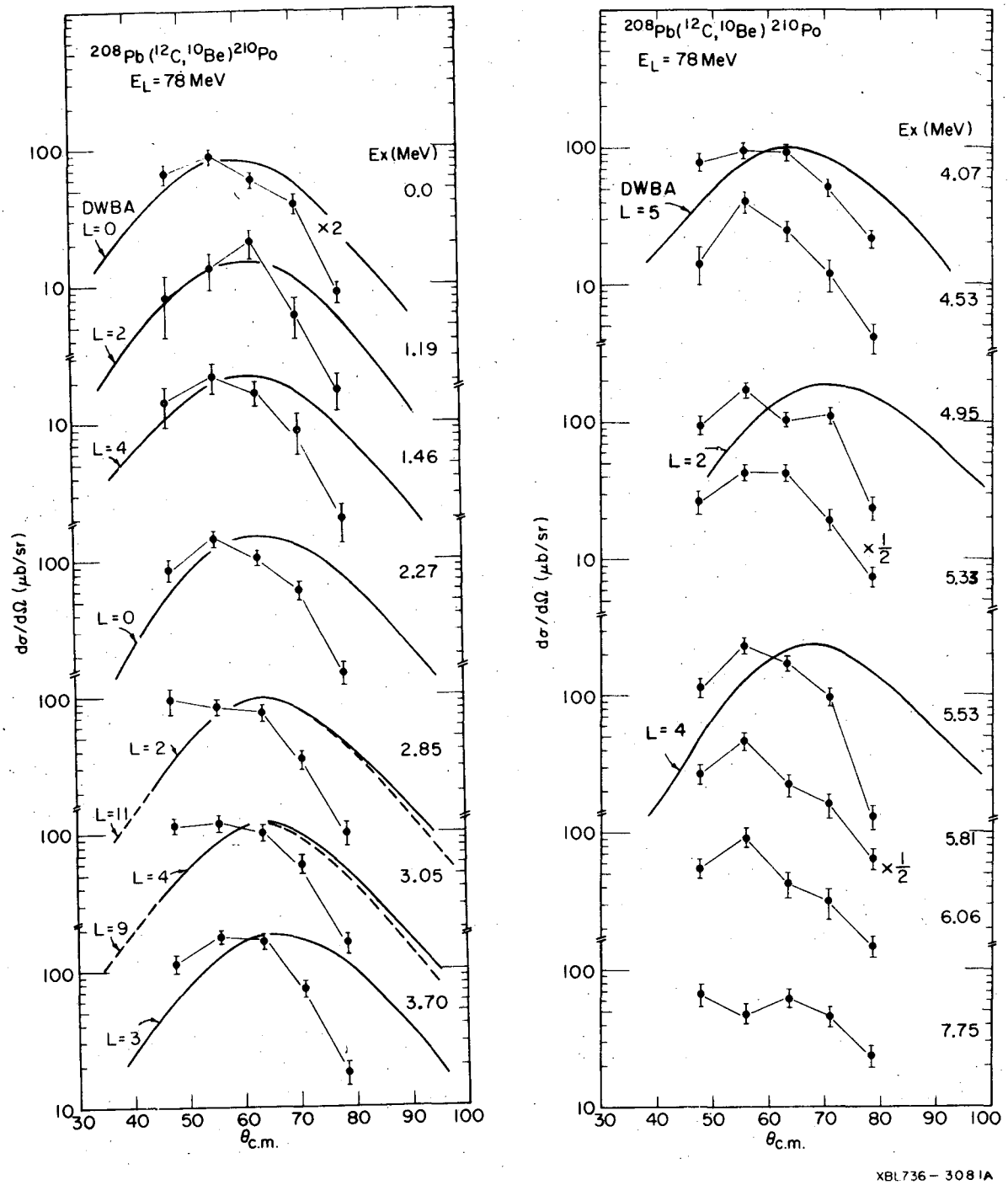
208Pb(12C,10Be)210Po
EL = 78 MeV
Ex (MeV)
0.0
1.19
1.46
2.27
2.85
3.05
3.70
DWBA
L=0
L=2
L=4
L=0
L=2
L=11
L=4
L=9
L=3
×2
dσ/dΩ (μb/sr)
θc.m.
208Pb(12C,10Be)210Po
EL = 78 MeV
Ex (MeV)
4.07
4.53
4.95
5.33
5.53
5.81
6.06
7.75
DWBA
L = 5
L = 2
L = 4
×1/2
×1/2
dσ/dΩ (μb/sr)
θc.m.
XBL736-3081A

Fig. 6

6

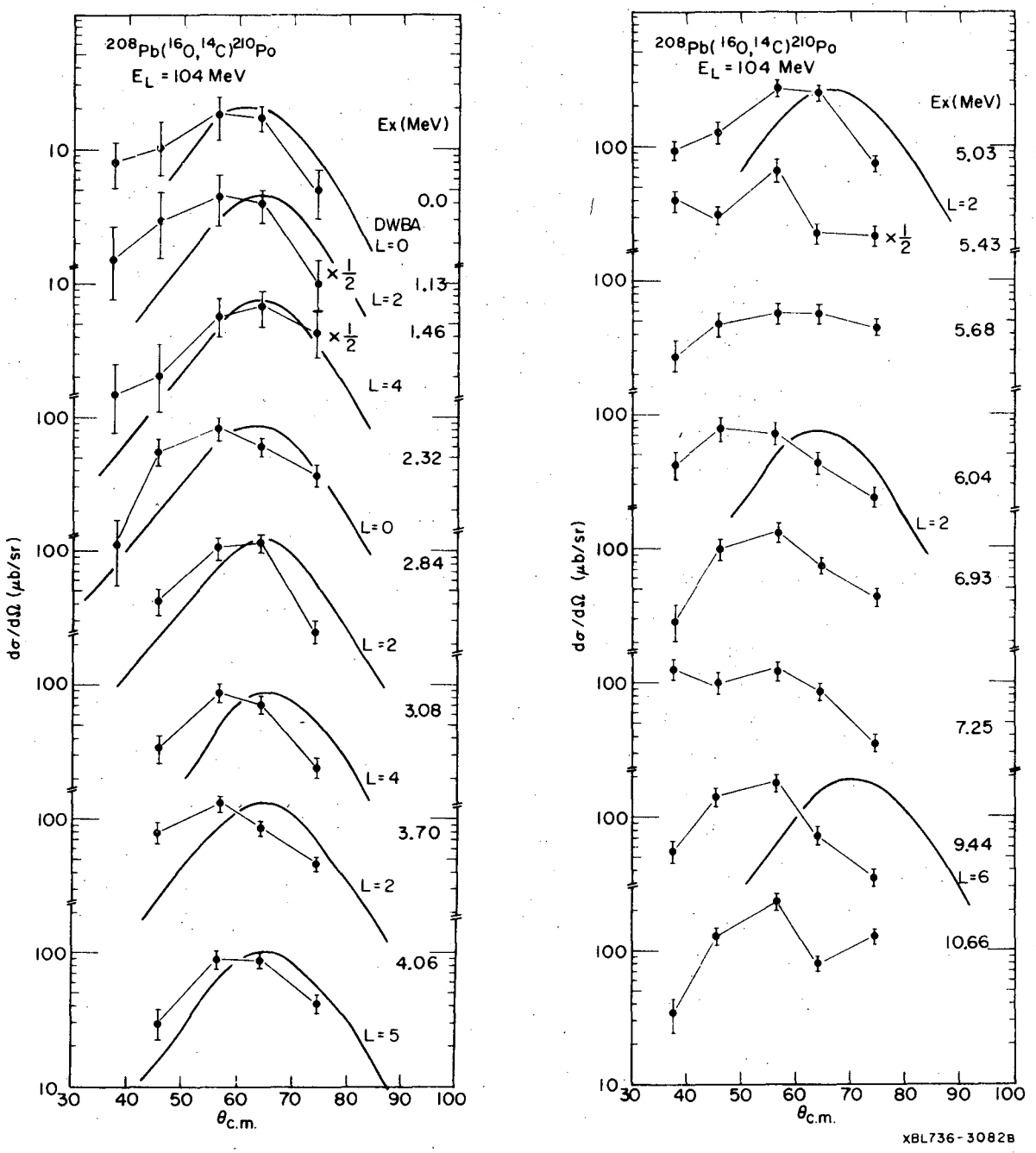
$^{208}Pb(^{16}O,^{14}C)^{210}Po$
E_L = 104 MeV
Ex (MeV)
0.0
DWBA
L=0
1.13
L=2
1.46
L=4
2.32
L=0
2.84
L=2
3.08
L=4
3.70
L=2
4.06
L=5
$\times\frac{1}{2}$
$d\sigma/d\Omega$ (μb/sr)
$\theta_{c.m.}$
5.03
L=2
5.43
5.68
6.04
L=2
6.93
7.25
9.44
L=6
10.66
XBL736-3082B

Fig. 7

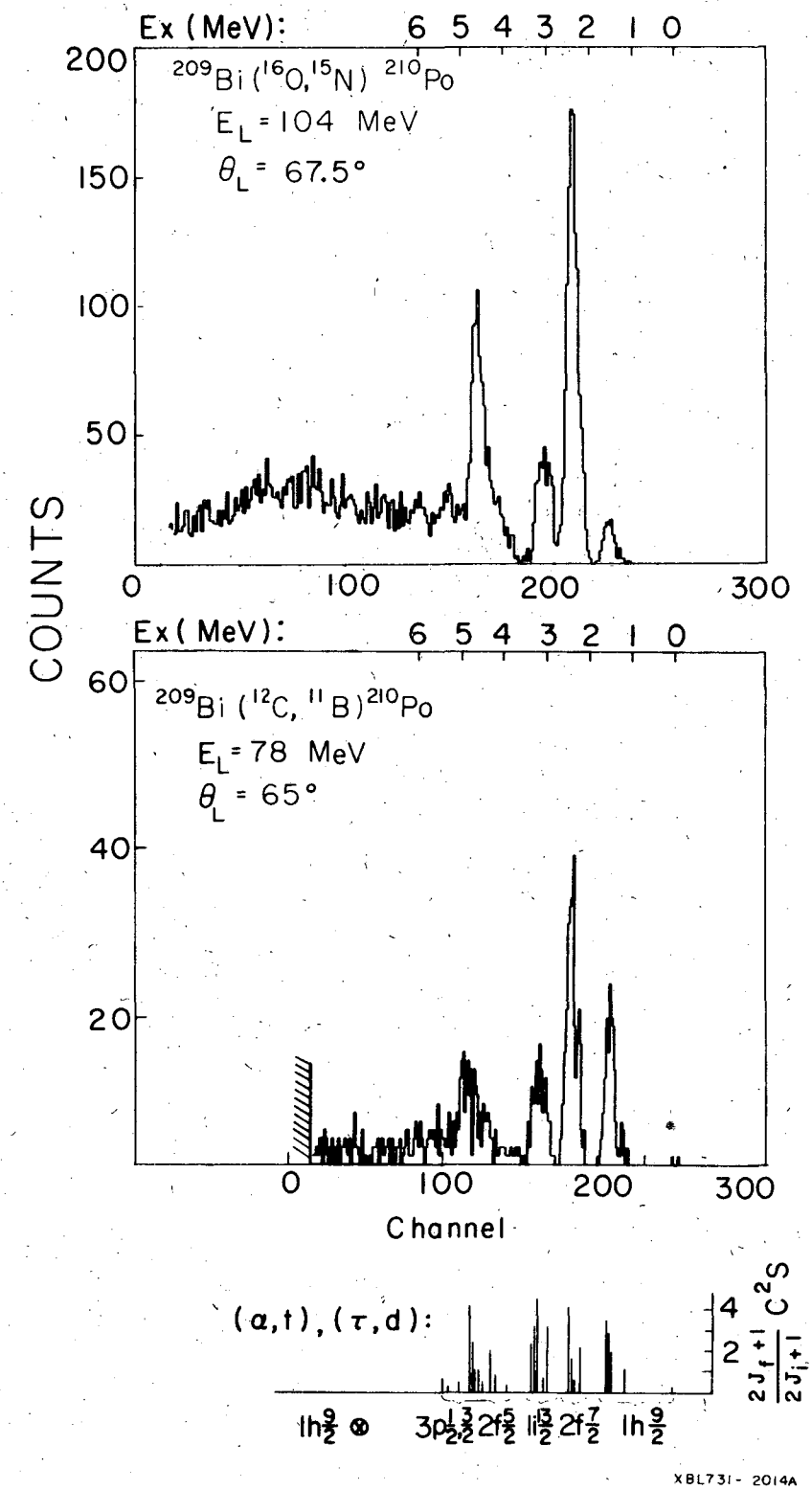
Ex (MeV): 6 5 4 3 2 1 0
^{209}Bi(^{16}O,^{15}N) ^{210}Po
E_L = 104 MeV
θ_L = 67.5°
COUNTS
Ex (MeV): 6 5 4 3 2 1 0
^{209}Bi (^{12}C, ^{11}B)^{210}Po
E_L = 78 MeV
θ_L = 65°
Channel
(α,t), (τ,d):
C^2S
$\frac{2J_f+1}{2J_i+1}$
$1h\frac{9}{2} \otimes$ $3p\frac{1}{2},\frac{3}{2}$ $2f\frac{5}{2}$ $1i\frac{13}{2}$ $2f\frac{7}{2}$ $1h\frac{9}{2}$
XBL731-2014A

Fig. 8

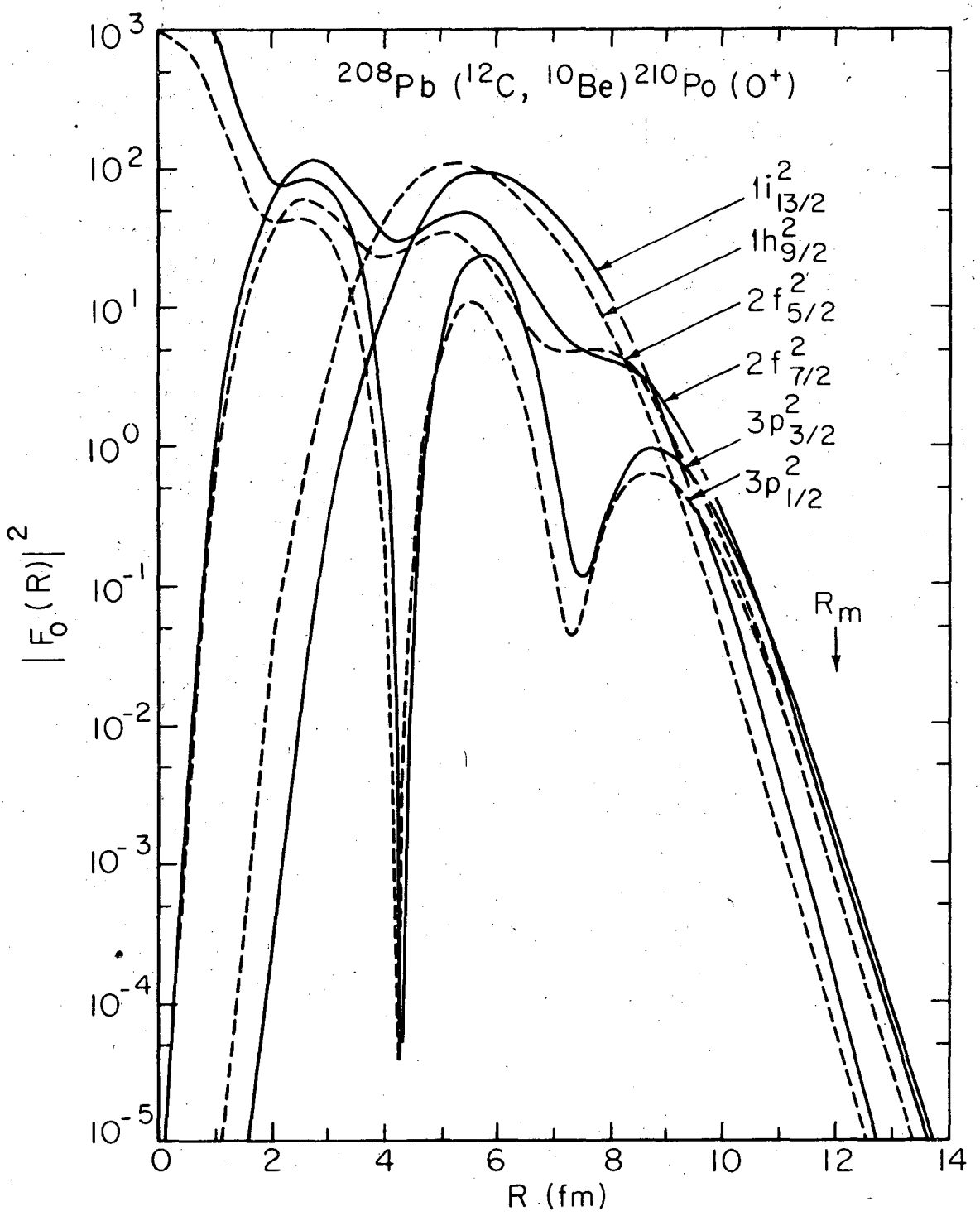

XBL736-3077A

Fig. 9

9

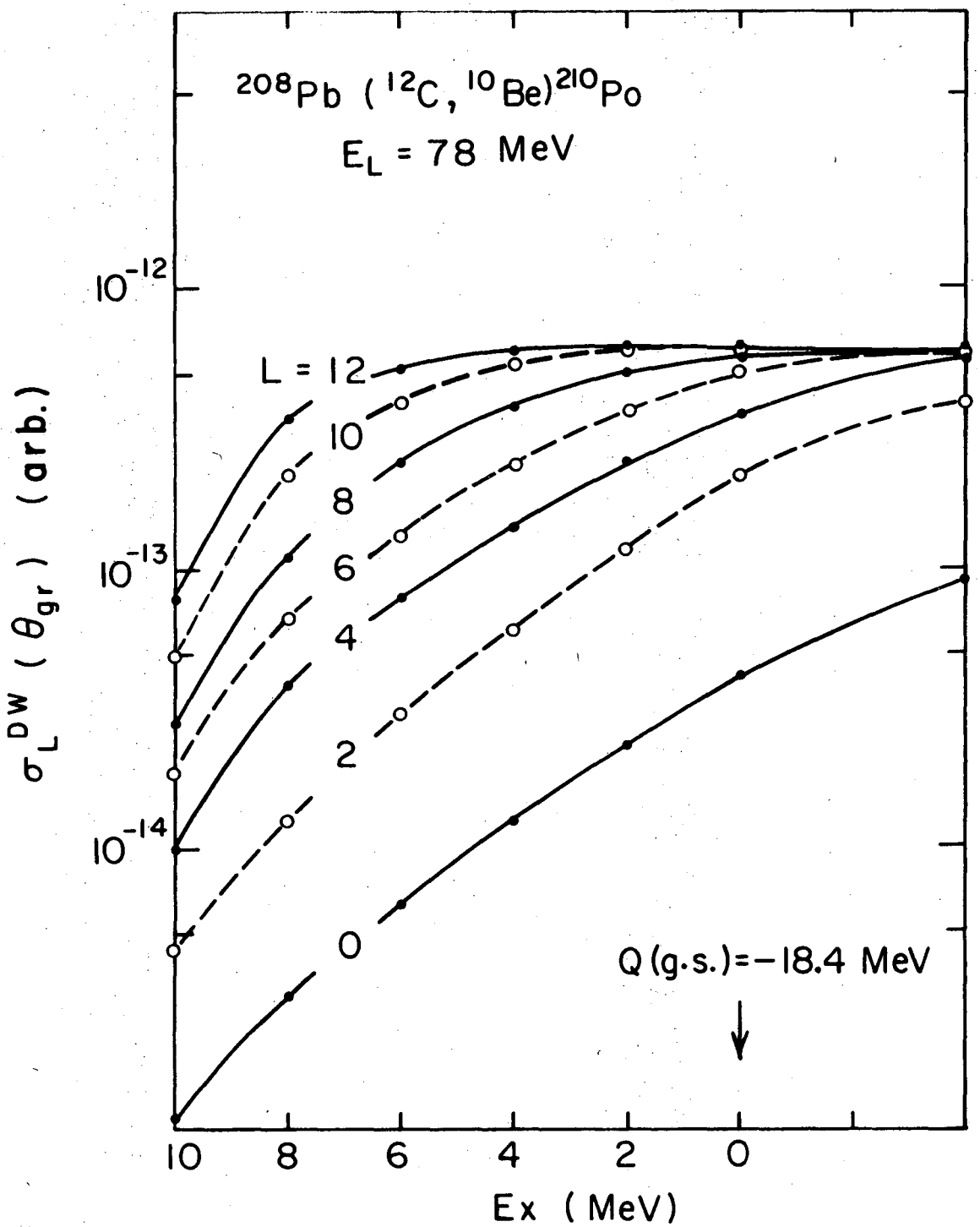

XBL735-2907

Fig. 10

10

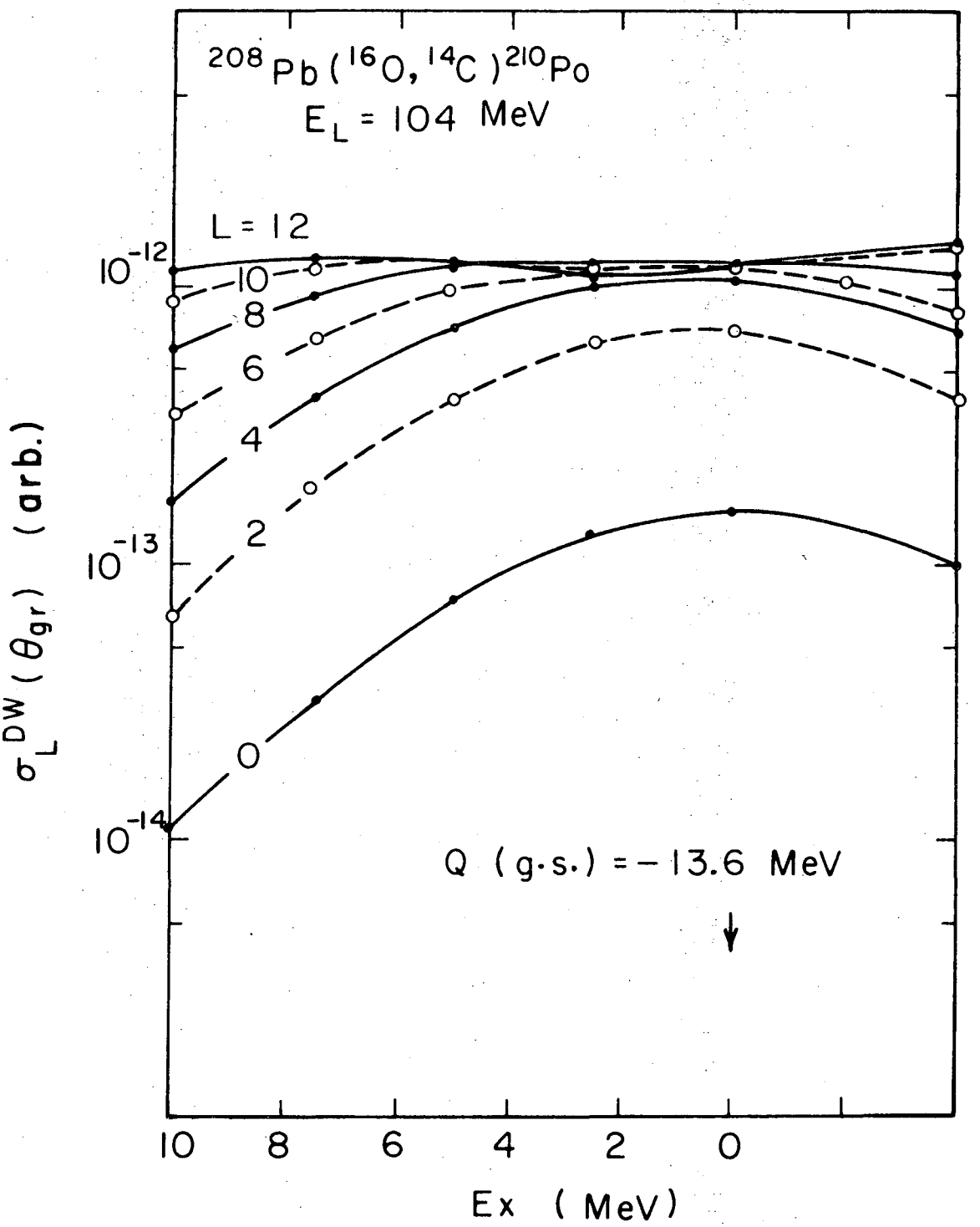

XBL735-2908

Fig. 11

11

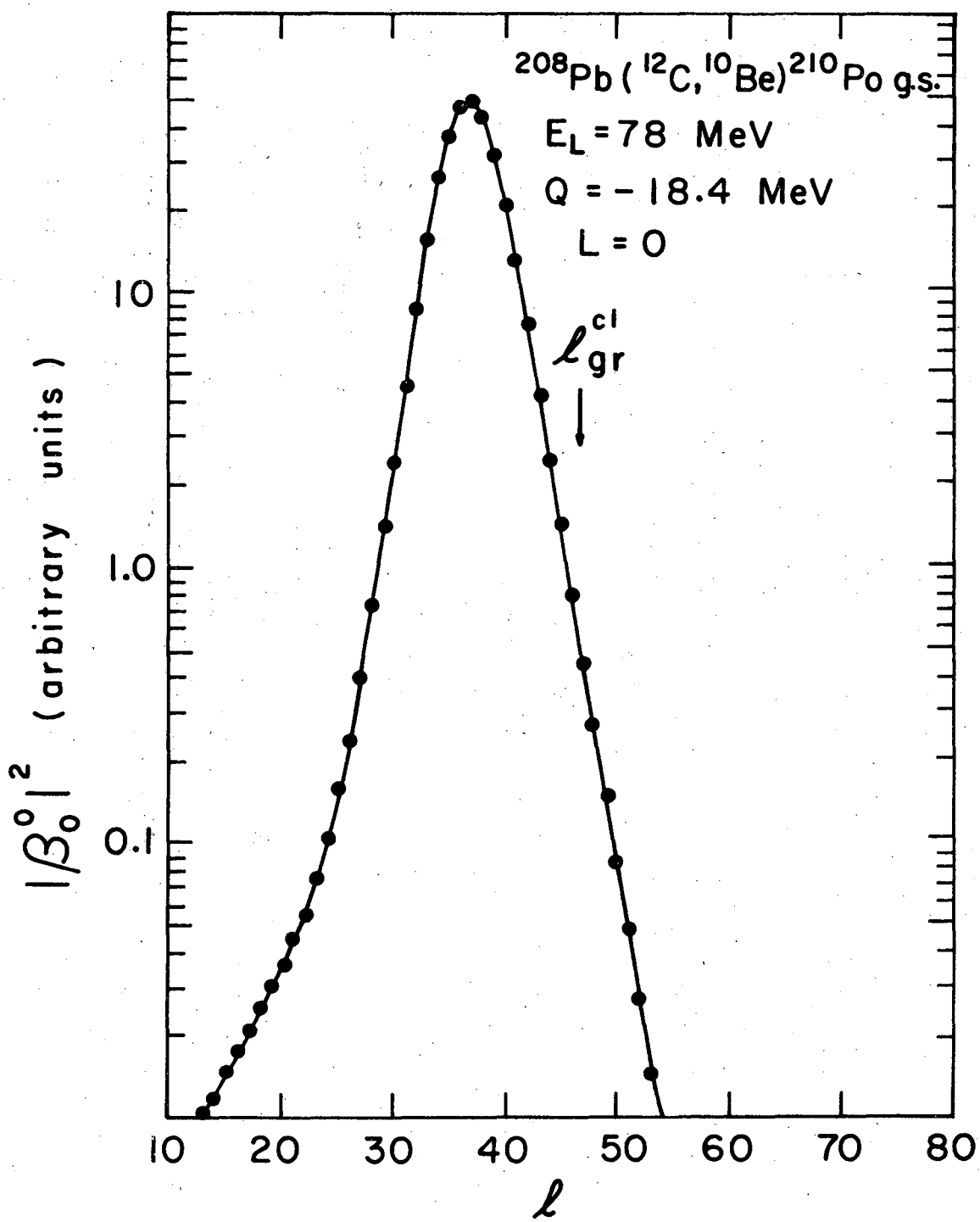

XBL 736-3162

Fig. 12

12

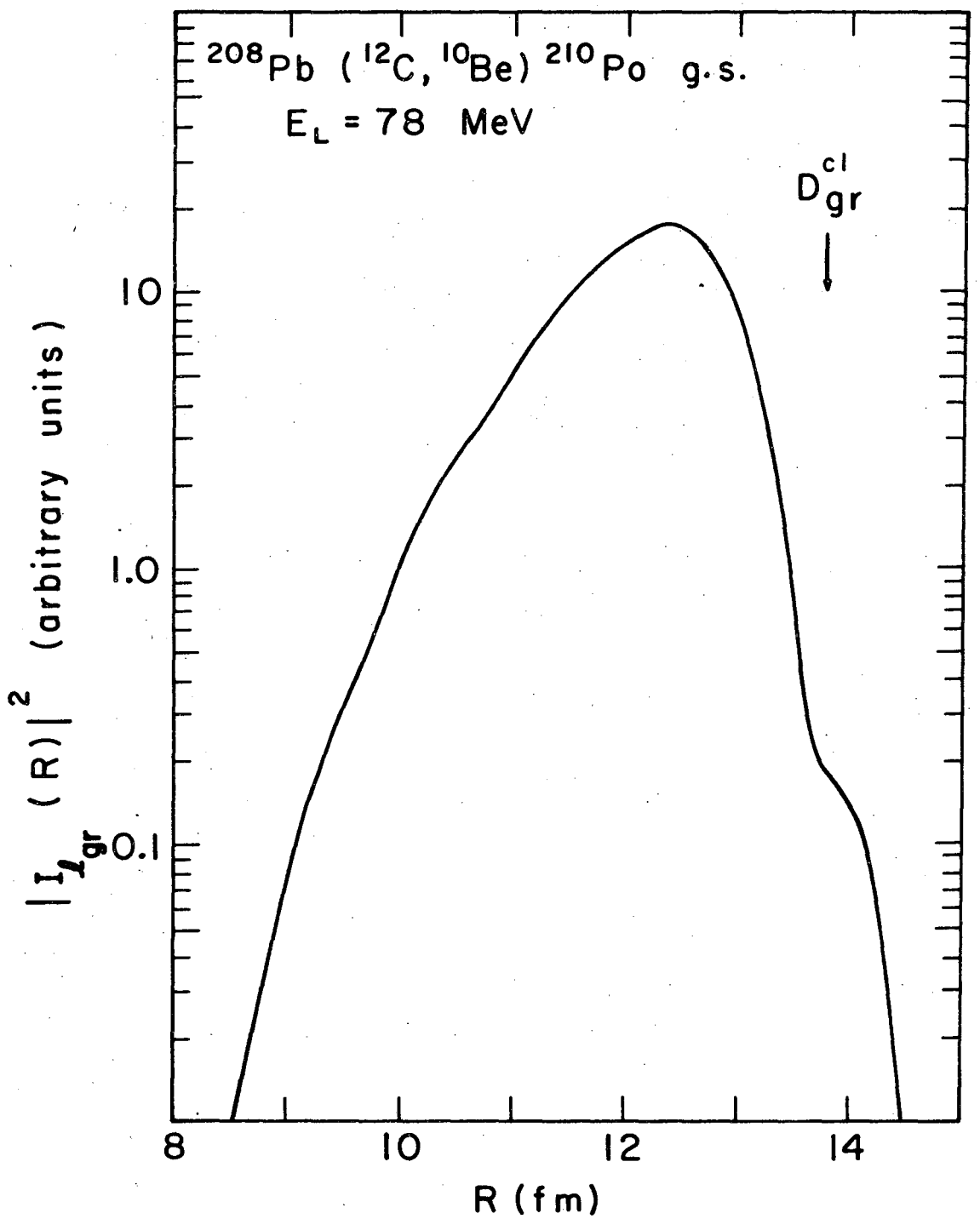

XBL 736-3161

Fig. 13

13

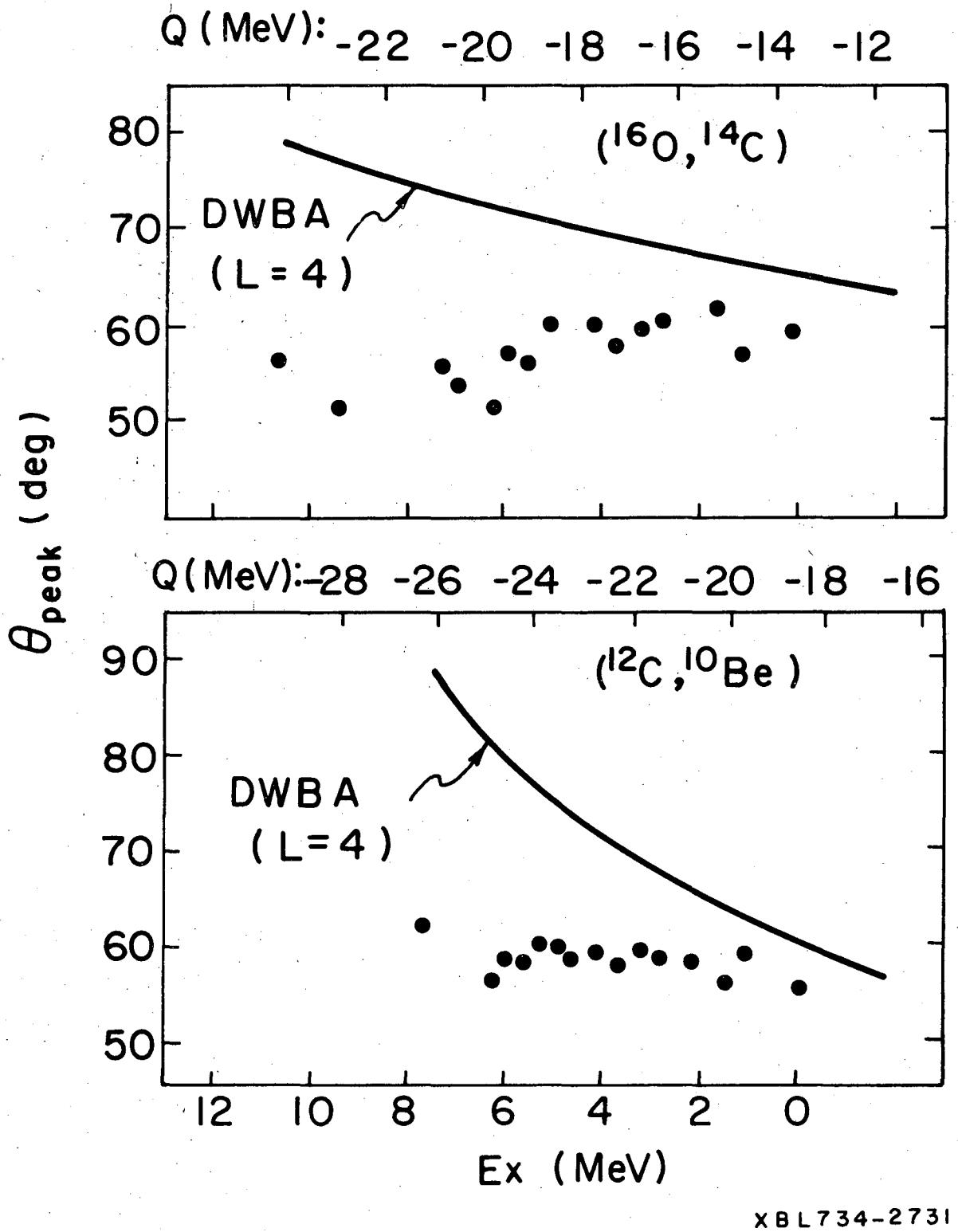
Q (MeV): -22 -20 -18 -16 -14 -12
80
70
60
50
(^{16}O,^{14}C)
DWBA
(L = 4)
θ_{peak} (deg)
Q (MeV): -28 -26 -24 -22 -20 -18 -16
90
80
70
60
50
(^{12}C,^{10}Be)
DWBA
(L=4)
12 10 8 6 4 2 0
Ex (MeV)
XBL734-2731

Fig. 14

14

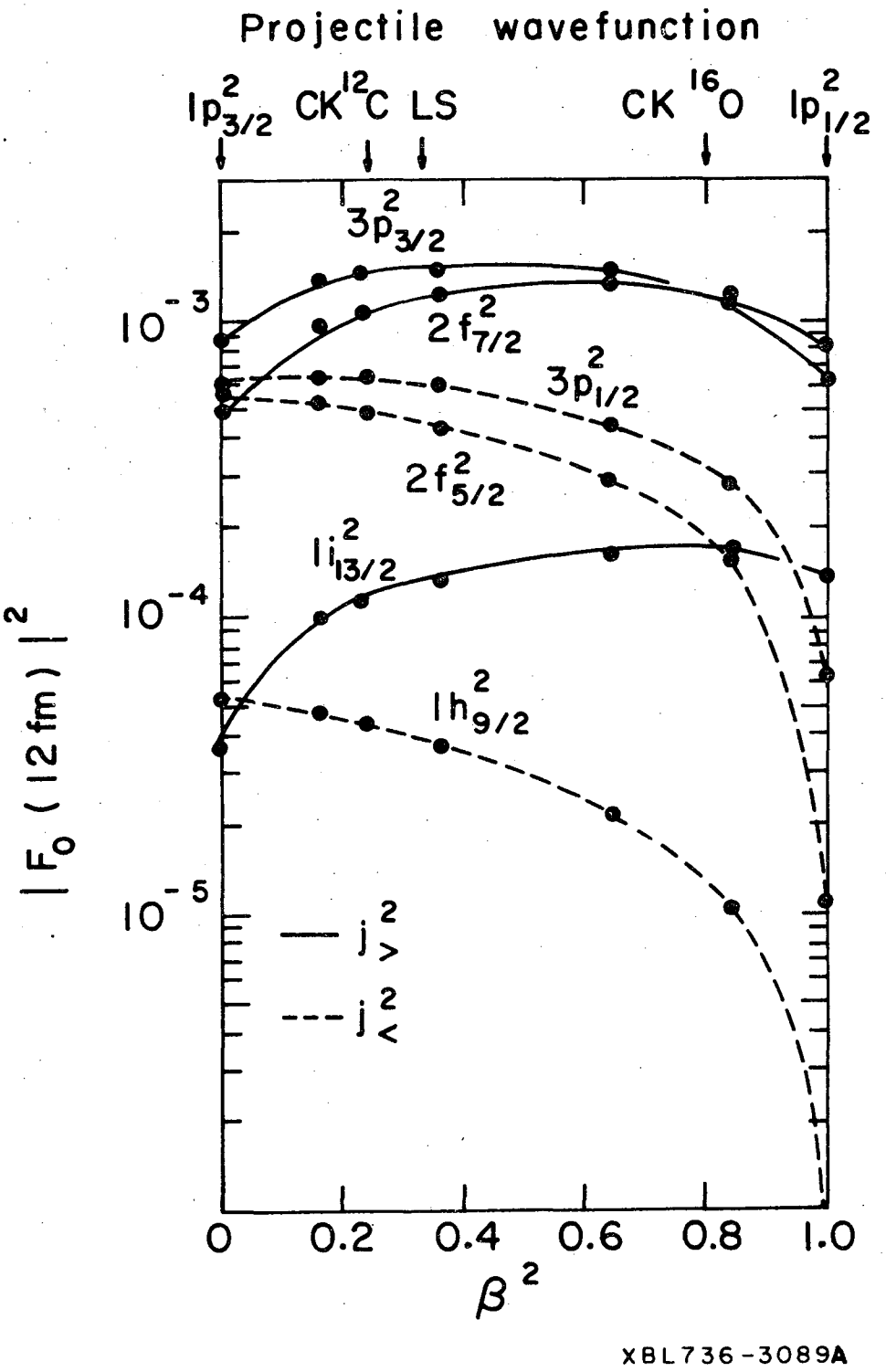
Projectile wavefunction
$1p^2_{3/2}$ CK ^{12}C LS CK ^{16}O $1p^2_{1/2}$
$3p^2_{3/2}$
$2f^2_{7/2}$
$3p^2_{1/2}$
$2f^2_{5/2}$
$1i^2_{13/2}$
$1h^2_{9/2}$
10^{-3}
10^{-4}
10^{-5}
$|F_0(12\,fm)|^2$
$j^2_>$
$j^2_<$
0 0.2 0.4 0.6 0.8 1.0
β^2
XBL736-3089A

Fig. 15

15

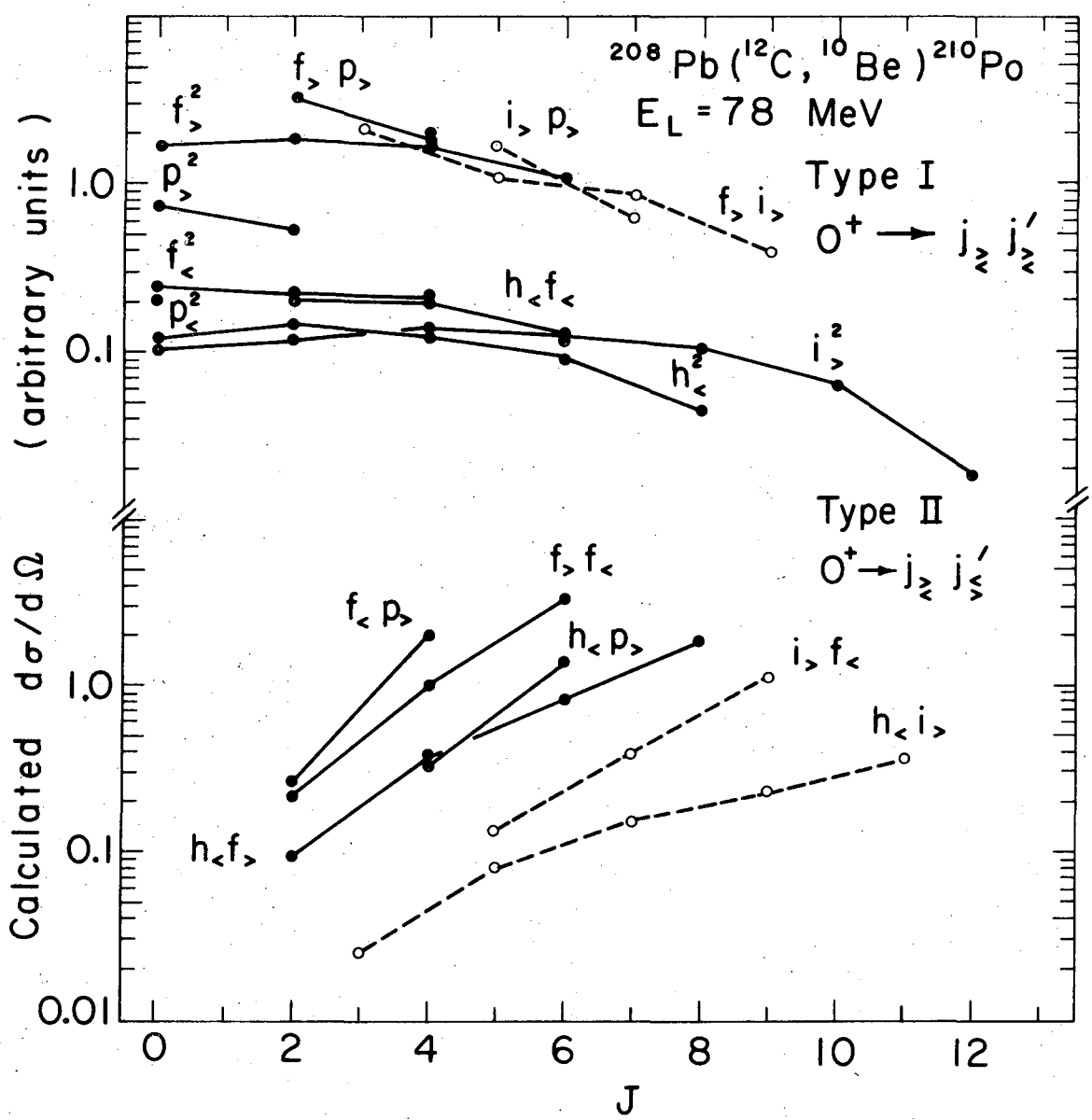

XBL736-3088

Fig. 16

16

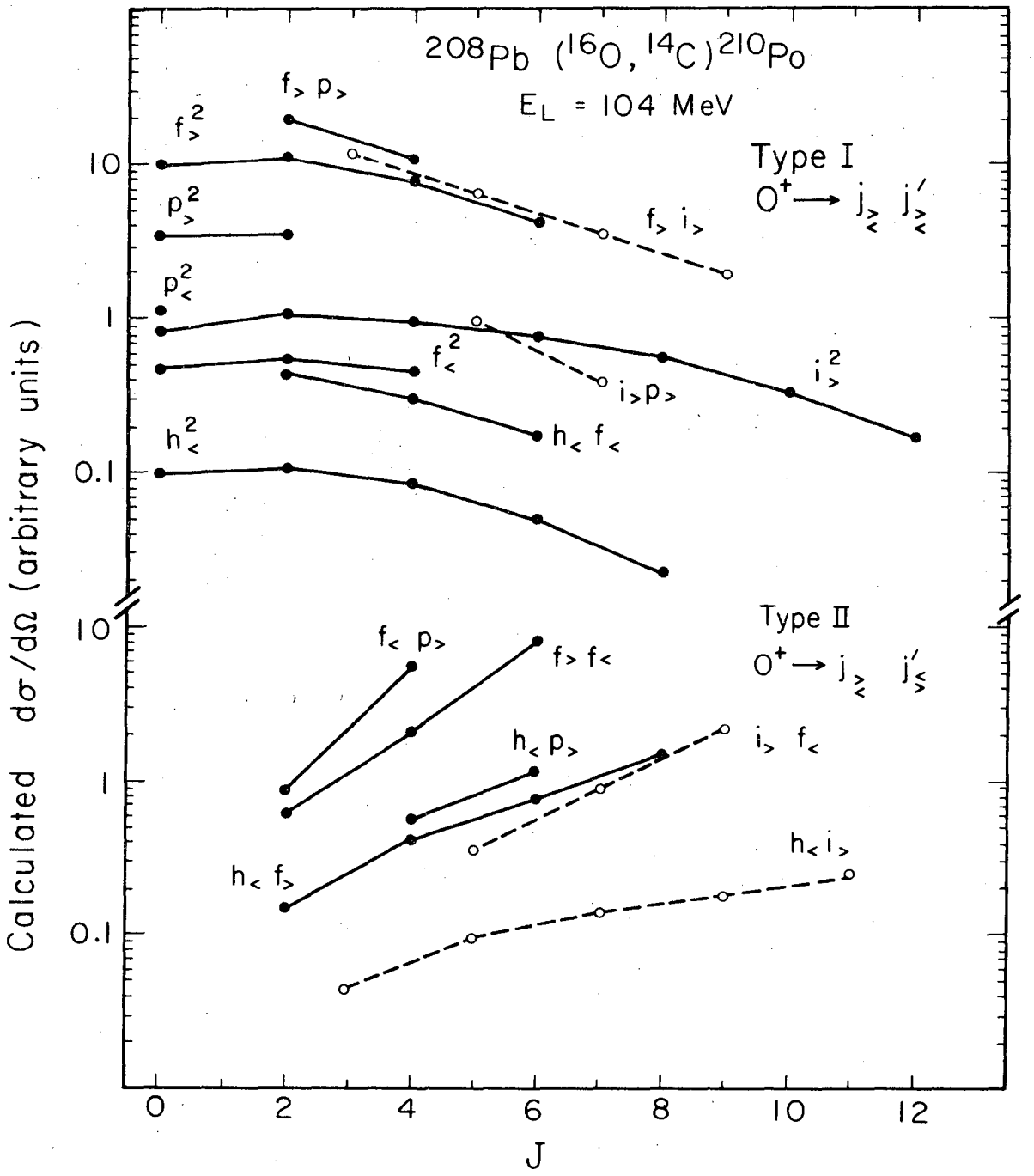
208Pb (16O, 14C)210Po
EL = 104 MeV
Type I
O+ → j≷ j'≷
Type II
O+ → j≷ j'≶
f> p>
f>2
p>2
p<2
f>2
f> i>
i>p>
i>2
h<2
h< f<
f< p>
f> f<
h< p>
i> f<
h< f>
h< i>
Calculated dσ/dΩ (arbitrary units)
J
XBL736-3083A

Fig. 17

17

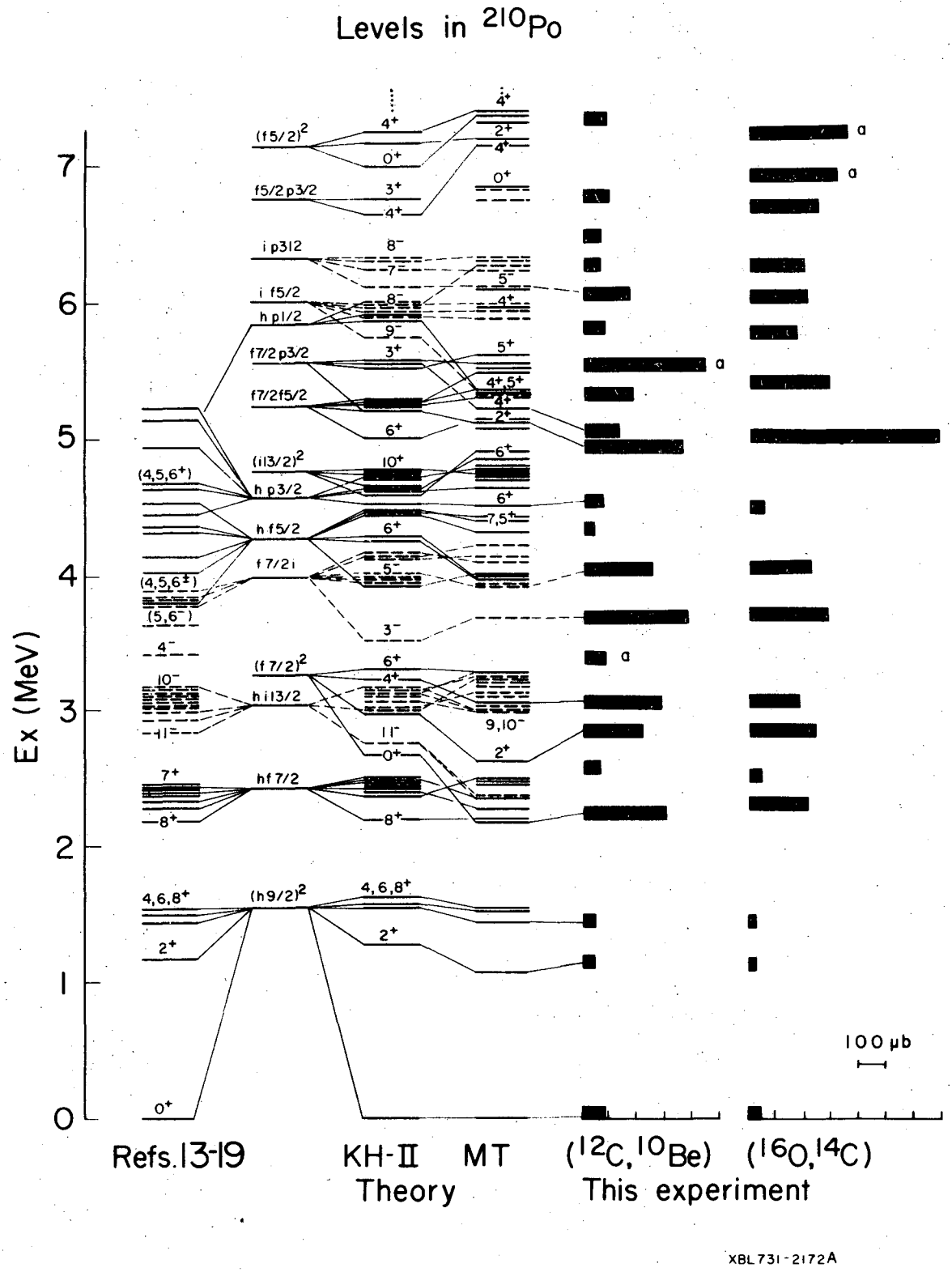
Levels in 210Po
Ex (MeV)
0
1
2
3
4
5
6
7
(f5/2)2
f5/2 p3/2
i p3/2
i f5/2
h p1/2
f7/2 p3/2
f7/2 f5/2
(i13/2)2
h p3/2
h f5/2
f 7/2 i
(f 7/2)2
h i13/2
hf 7/2
(h9/2)2
(4,5,6+)
(4,5,6±)
(5,6−)
4−
10−
11−
7+
8+
4,6,8+
2+
0+
a
100 μb
Refs.13-19
KH-II
MT
Theory
(12C,10Be)
(16O,14C)
This experiment
XBL 731-2172A

Fig. 18

18

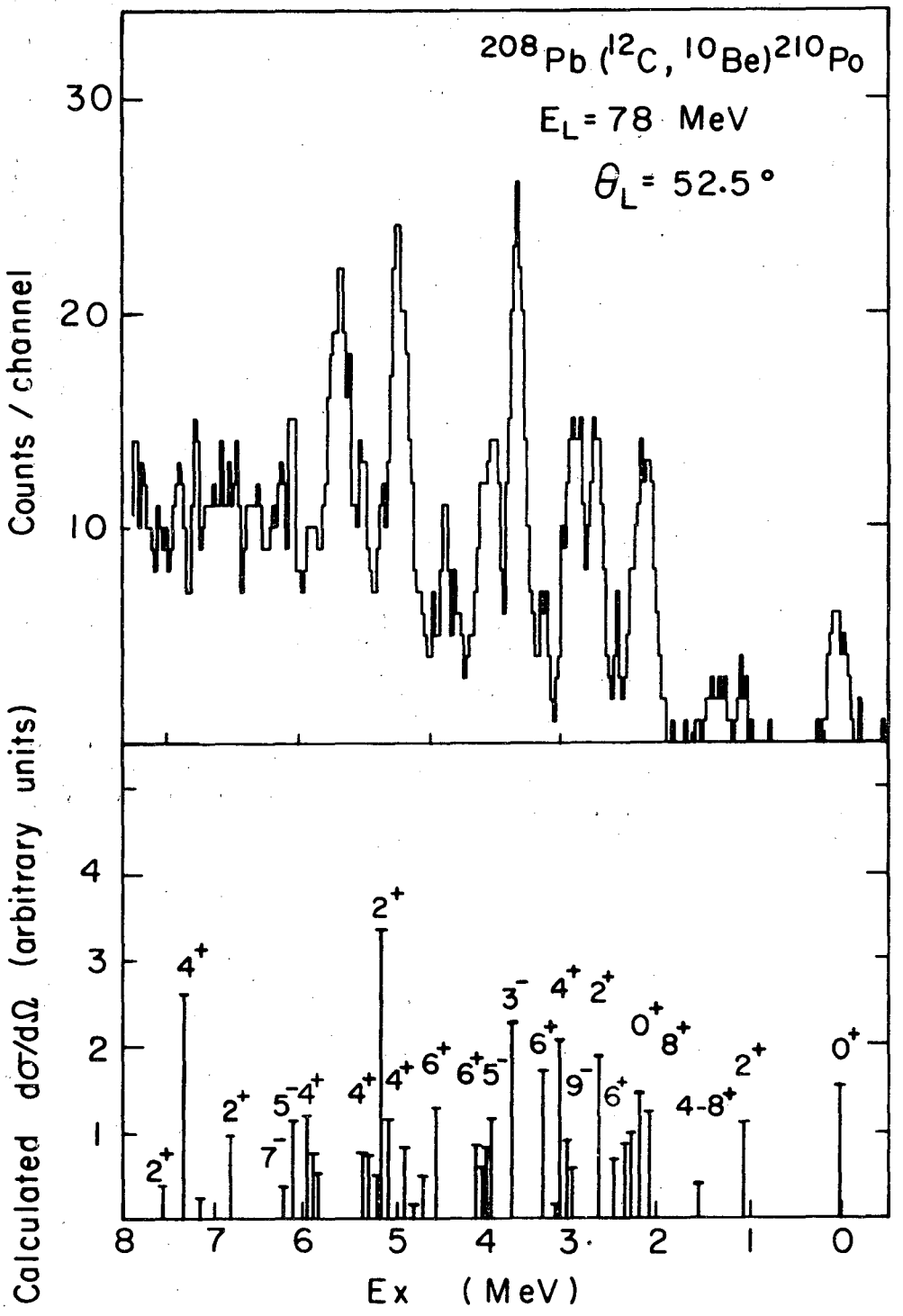

XBL736-3080A

Fig. 19

19

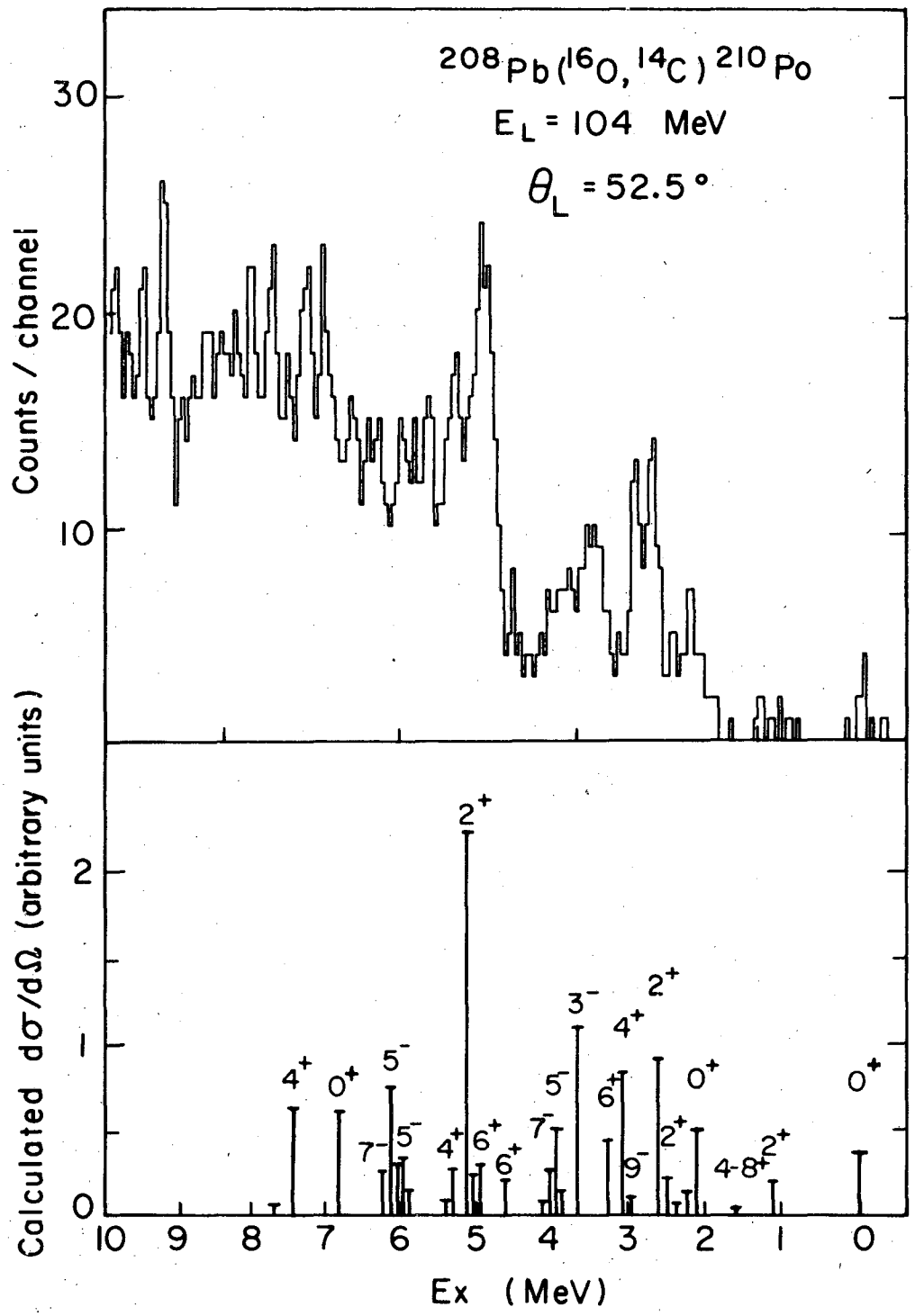

XBL736-3079A

Fig. 20

20

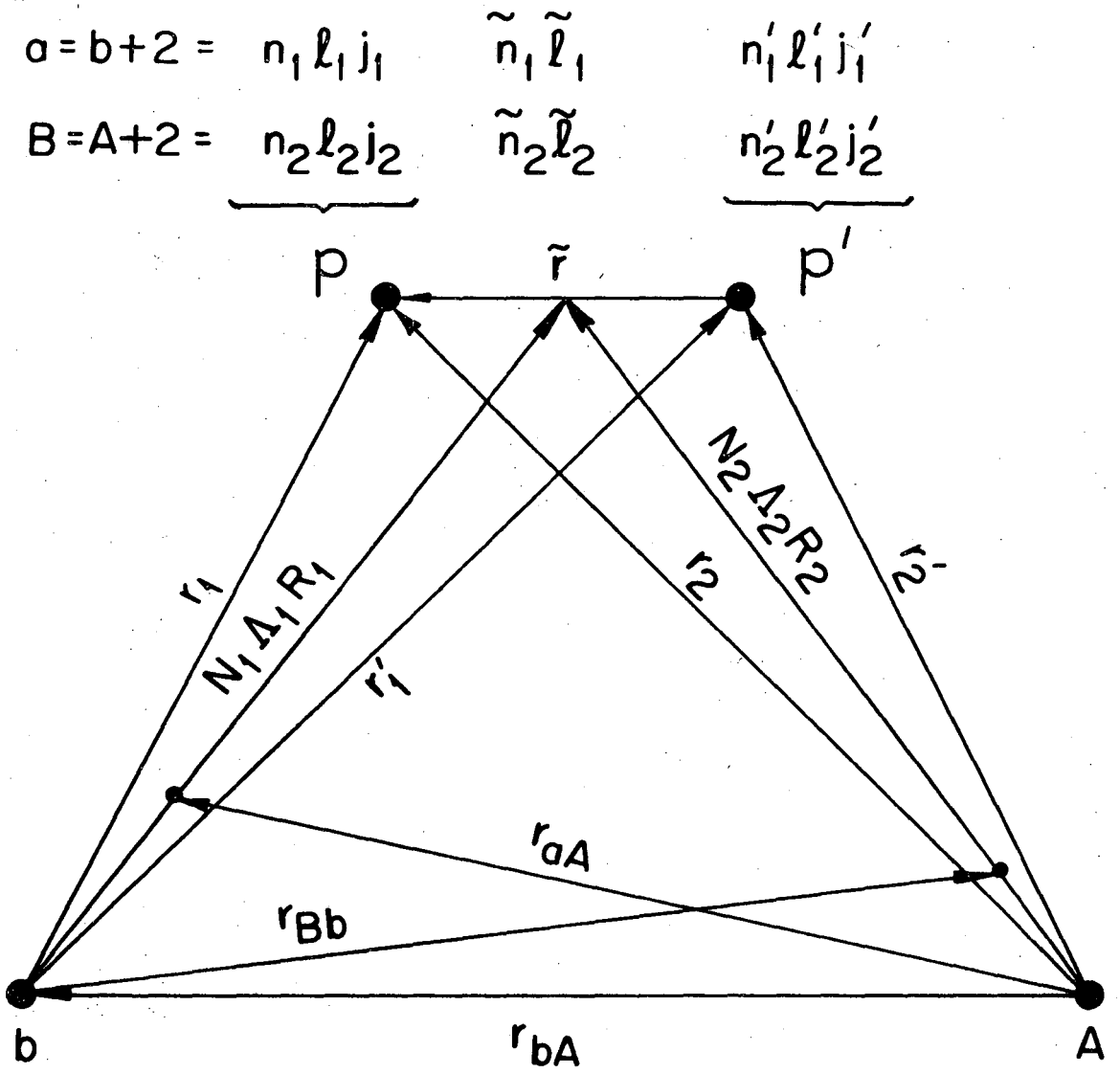

XBL731-2174A

Fig. 21

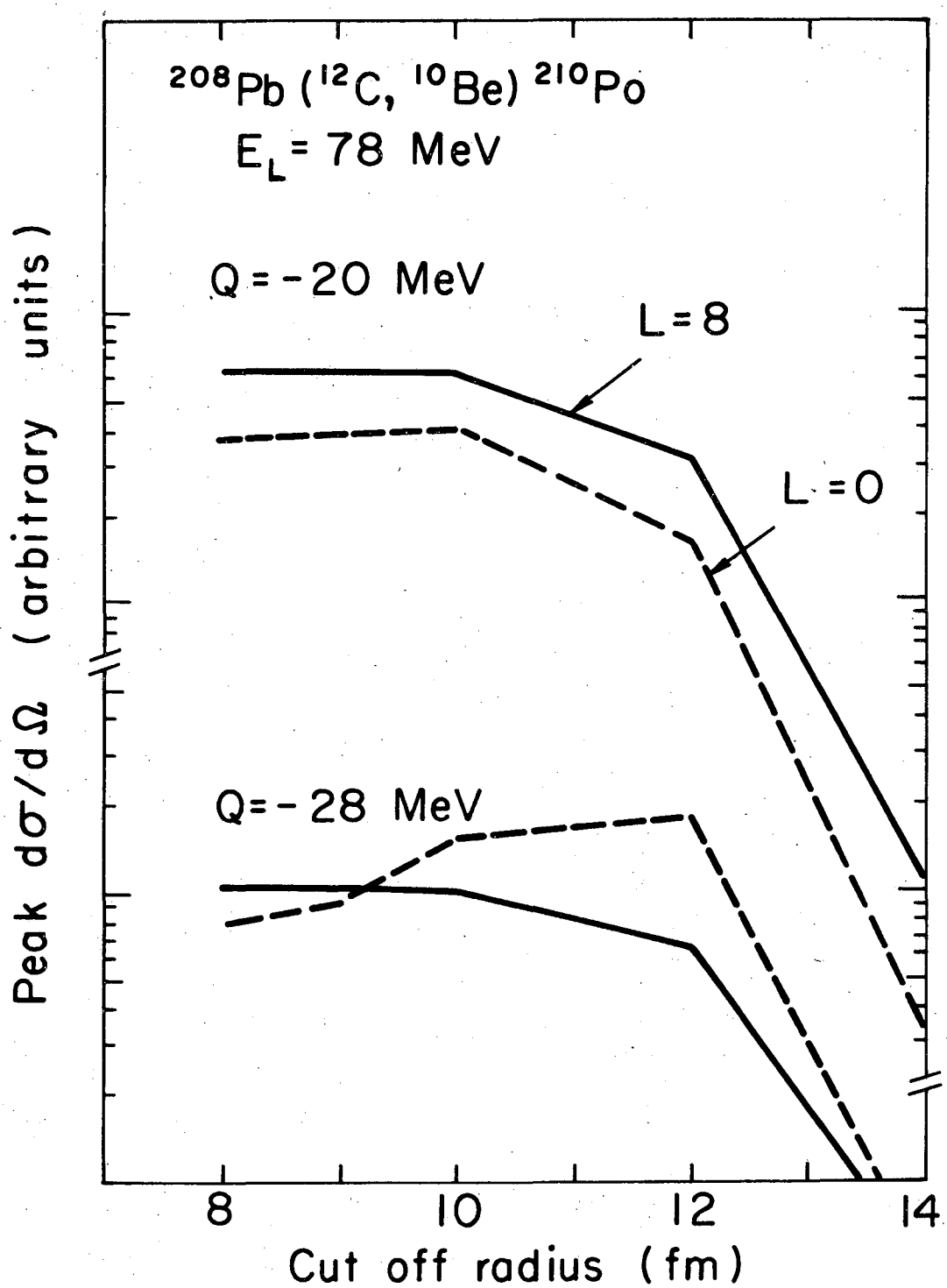

XBL732-2320

Fig. 22

22

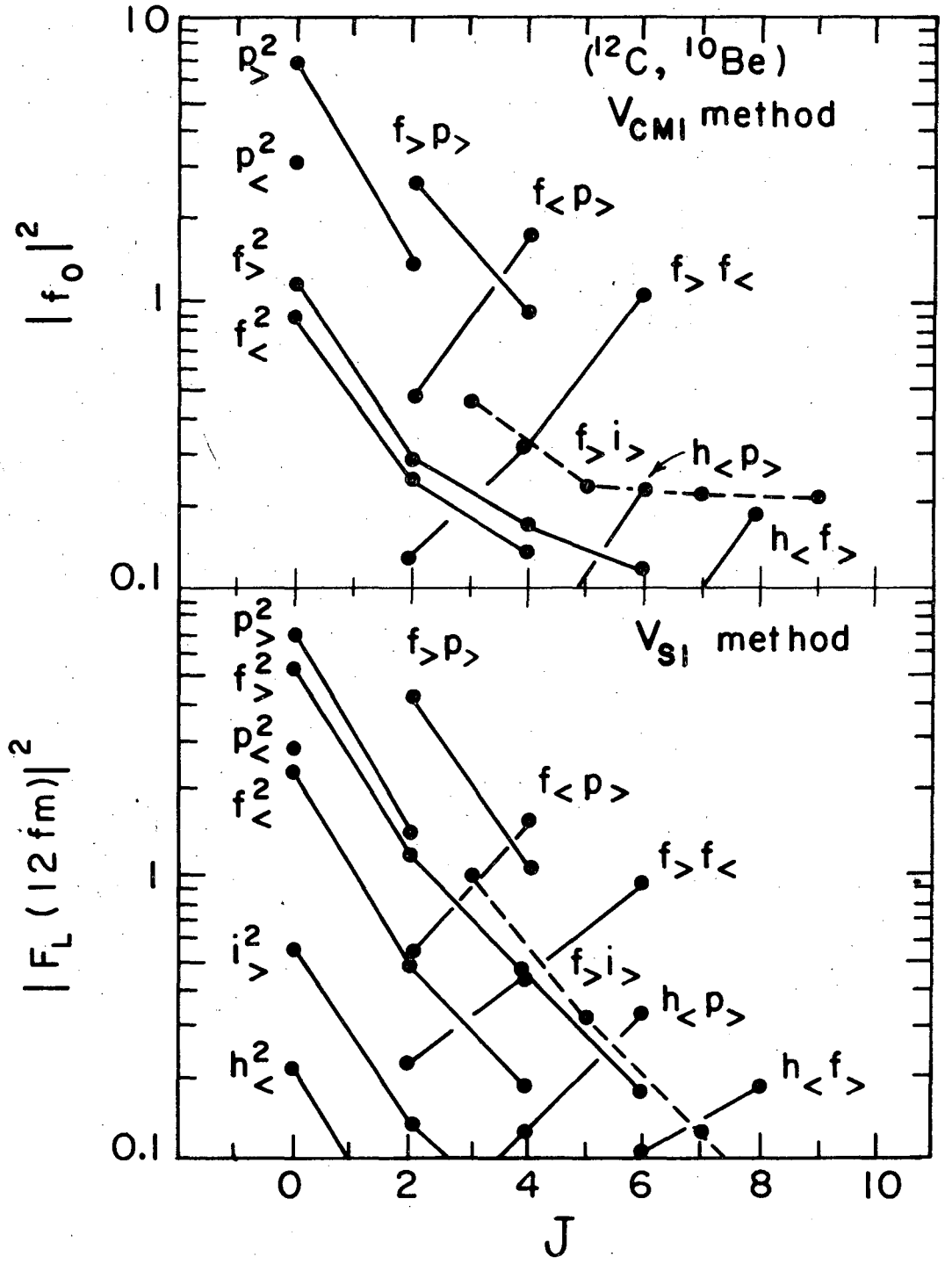

XBL736-3090A

Fig. 23

LEGAL NOTICE

This report was prepared as an account of work sponsored by the United States Government. Neither the United States nor the United States Atomic Energy Commission, nor any of their employees, nor any of their contractors, subcontractors, or their employees, makes any warranty, express or implied, or assumes any legal liability or responsibility for the accuracy, completeness or usefulness of any information, apparatus, product or process disclosed, or represents that its use would not infringe privately owned rights.

TECHNICAL INFORMATION DIVISION
LAWRENCE BERKELEY LABORATORY
UNIVERSITY OF CALIFORNIA
BERKELEY, CALIFORNIA 94720